Towards a multi-platform assimilative system for North Sea biogeochemistry

Jozef Skákala[1,2], David Ford[3], Jorn Bruggeman[1], Tom Hull[4,5], Jan Kaiser[5], Robert R. King[3], Benjamin Loveday[1], Matthew R. Palmer[6], Tim Smyth[1], Charlotte A. J. Williams[6]and Stefano Ciavatta[1,2]

[1]Plymouth Marine Laboratory, The Hoe, Plymouth, PL1 3DH United Kingdom.
[2]National Centre for Earth Observation, Plymouth, PL1 3DH, UK.
[3]Met Office, FitzRoy Road, Exeter, EX1 3PB UK.
[4]Centre for Environment, Fisheries and Aquaculture Science, Lowestoft, NR33 0HT UK.
[5]Centre for Ocean and Atmospheric Sciences, University of East Anglia, Norwich, NR4 7TJ, UK.
[6]National Oceanography Centre, Joseph Proudman Building, 6 Brownlow Street, Liverpool, L3 5DA UK.

Key Points:

- We successfully developed a multi-platform assimilative system for biogeochemistry in the North Sea.
- We tested the impact of the different assimilative system components on the ecosystem reanalysis.
- The multi-platform assimilation will become an essential part of future operational research.

Corresponding author: Jozef Skákala, jos@pml.ac.uk

Abstract

Oceanography has entered an era of new observing platforms, such as biogeochemical Argo floats and gliders, some of which will provide three-dimensional maps of essential ecosystem variables on the North-West European (NWE) Shelf. In a foreseeable future operational centres will use multi-platform assimilation to integrate those valuable data into ecosystem reanalyses and forecast systems. Here we address some important questions related to glider biogeochemical data assimilation and introduce multi-platform data assimilation in a (pre)operational model of the NWE Shelf-sea ecosystem. We test the impact of the different multi-platform system components (glider vs satellite, physical vs biogeochemical) on the simulated biogeochemical variables. To characterize the model performance we focus on the period around the phytoplankton spring bloom, since the bloom is a major ecosystem driver on the NWE Shelf. We found that the timing and magnitude of the phytoplankton bloom is insensitive to the physical data assimilation, which is explained in the study. To correct the simulated phytoplankton bloom one needs to assimilate chlorophyll observations from glider or satellite Ocean Color (OC) into the model. Although outperformed by the glider chlorophyll assimilation, we show that OC assimilation has mostly desirable impact on the sub-surface chlorophyll. Since the OC assimilation updates chlorophyll only in the mixed layer, the impact on the sub-surface chlorophyll is the result of the model dynamical response to the assimilation. We demonstrate that the multi-platform assimilation combines the advantages of its components and always performs comparably to its best performing component.

Plain Language Summary

North-West European (NWE) Shelf is a region of major importance for both European economy and climate. Observational oceanography has entered an important era of new observing biogeochemical platforms, such as Biogeochemical Argos and gliders. Gliders are being currently deployed to measure three-dimensional distributions of some essential biogeochemical variables on the NWE Shelf. This work establishes a multi-platform assimilative system on the NWE Shelf which will be used to combine multiple different types of observing platforms (e.g. satellite, gliders) with our up-to-date models in order to optimize our estimate and forecast of the NWE Shelf ecosystem state. We provide an understanding for how the different components of the system interact. We demonstrate that the assimilative system is skilled to combine physical data with satellite and glider data for chlorophyll, as well as the glider data for oxygen. The work establishes the foundations of a system that is planned to be used in the future operational oceanography on the NWE Shelf.

1 Introduction

Understanding the state and the future of shelf-sea ecosystems is essential from the point of view of economy, conservation and the global carbon cycle (*Pauly et al.* [2002]; *Borges et al.* [2006]; *Friedlingstein et al.* [2006]; *Jahnke* [2010]). Reanalyses provide our best estimate of the ocean state by optimally combining the state-of-the-art knowledge from models with the most up-to-date observations. In marine biogeochemistry the prevailing approach is to assimilate satellite products into models, either for Ocean Color (OC) derived total chlorophyll (e.g *Ishizaka* [1990]; *Carmillet et al.* [2001]; *Natvik and Evensen* [2003]; *Hoteit et al.* [2005]; *Triantafyllou et al.* [2007]; *Nerger and Gregg* [2007, 2008]; *Gregg* [2008]; *Fontana et al.* [2010]; *Ford et al.* [2012]; *Ciavatta et al.* [2011, 2016]; *Kalaroni et al.* [2016]; *Ford and Barciela* [2017]; *Pradhan et al.* [2019]), Phytoplankton Functional Type (PFT)-specific chlorophyll (*Ciavatta et al.* [2018, 2019]; *Skákala et al.* [2018, 2020]), or surface radiances (*Shulman et al.* [2013]; *Ciavatta et al.* [2014]; *Jones et al.* [2016]; *Gregg and Rousseaux* [2017]; *Skákala et al.* [2020]). Additionally a number of studies have assimilated biogeochemical data from in situ measurements, either using

single-location profiles (e.g. *Allen et al.* [2003]; *Hoteit et al.* [2003]; *Torres et al.* [2006]; *Lenartz et al.* [2007]), or using surface data from ships, floats and buoys (e.g *Anderson et al.* [2000]; *Cossarini et al.* [2009]; *Song et al.* [2016]). The typical disadvantage of the traditionally assimilated biogeochemical data-sets is that they are either constrained to the ocean surface (e.g. in the case of satellite data), or they are typically limited to a single location (in the case of vertically-measured data). Assimilating such data into the model has either only local impact, or its impact on biogeochemical fields is typically constrained to the upper oceanic layer, with uncertain impact on the vertical profiles of biomass, or nutrients.

However, the situation on the data-front is rapidly changing, with new programmes (e.g. AtlantOS, *Visbeck et al.* [2015]) aiming at revolutionizing biogeochemical oceanography with novel observing platforms covering large parts of the ocean both horizontally and vertically, such as floats deployed in the Biogeochemical-Argo programme (e.g. *Johnson and Claustre* [2016]; *Johnson* [2016]; *Germineaud et al.* [2019]), and gliders with optical and biogeochemical sensors (*Telszewski et al.* [2018]). Some of the Argo float oxygen data were already assimilated to constrain the biogeochemistry in the Southern Ocean (*Verdy and Mazloff* [2017]) and Argo-measured chlorophyll was assimilated to improve phytoplankton dynamics in the Mediterranean Sea (*Cossarini et al.* [2019]). This new observational activity quite understandably focuses on regions of high importance for fisheries, economy and climate, such as the North-West European (NWE) Shelf (e.g. *Legge et al.* [2020]), where a number of gliders have been deployed as a part of the Alternative Framework to Assess Marine Ecosystem Functioning in Shelf Seas (AlterECO) programme (*http://projects.noc.ac.uk/altereco/*). The rapid development of these new autonomous observation systems opens up an entirely new range of possibilities on how to optimally integrate multi-platform observing networks with our present oceanographic models (*Lellouche et al.* [2013]; *Bell et al.* [2015]). The observational work on the NWE Shelf from the AlterECO project is coupled to a sister programme, the CAMPUS (Combining Autonomous observations and Models for Predicting and Understanding Shelf seas, *https://www.campus-marine.org/*) project, aiming to consistently combine the different sources of information, such as gliders, satellite OC data and models, in order to improve our capability to understand, represent and forecast the NWE Shelf biogeochemistry (e.g spring bloom, carbon and nutrient cycle, oxygen depletion events). Future plans, based on CAMPUS and in line with the European Copernicus Marine Environment Monitoring Service (CMEMS), are to have a multi-platform assimilative system on the NWE Shelf, where the autonomous vehicles will navigate to specific locations using a combination of Artificial Intelligence (AI) and model forecast, to observe important processes such as the onset of the phytoplankton bloom, or hypoxic events.

Trying to establish glider data assimilation as part of such a multi-platform assimilative system often leads to two non-trivial problems: a) how to consistently combine high resolution glider data with much coarser model resolution, b) how to achieve reasonable consistency between the assimilation-corrected variables and the coupled physical-biogeochemical model dynamics. The problem of dynamical consistency needs special mention, since both physical and biogeochemical fields have typically much larger gradients in the vertical than in the horizontal dimension. The vertical correlation length scales have large spatio-temporal variability and model dynamics can be quite sensitive to spurious vertical gradients (*Doney* [1999]; *Oschlies and Garçon* [1999]; *Doney et al.* [2004]). Such model sensitivity is often noticed when physical data (such as sea surface height, or temperature and salinity) are assimilated into the model, as the spurious vertical mixing introduced by such assimilation is known to often degrade the skill of the biogeochemical model (e.g *Berline et al.* [2007]; *While et al.* [2010]; *El Moussaoui et al.* [2011]; *Holt et al.* [2014]; *Raghukumar et al.* [2015]; *Park et al.* [2018]). However, similar issues can be easily overlooked when we assimilate surface biogeochemical data (except extreme regions with substantial small-scale horizontal variability, such as the Gulf Stream, *Anderson et al.* [2000]), since the biogeochemical fields have smaller gradients in the horizontal direction

than in the vertical, which means they are more dynamically stable in the horizontal than in the vertical direction. For the gliders, it is of vital interest to understand the potentially complex interaction between the physical and the biogeochemical data assimilation, or the interplay between the different biogeochemical variables updated by the assimilative system.

In this study we extend the operational assimilative system on the NWE Shelf to successfully produce a multi-platform reanalysis including both physical (satellite sea surface temperature, temperature and salinity from in situ platforms and an AlterEco glider) and biogeochemical (total chlorophyll *a* and oxygen from an AlterECO glider, and chlorophyll *a* from a satellite OC product) variables. The main focus of the paper is to assess the impact of the different multi-platform assimilative system components (satellite vs glider, physical vs biogeochemical) on the simulated ecosystem processes in relation to the phytoplankton spring bloom. Being able to estimate the impact of the different system components is important, since it indicates what the assimilation impact will be on the simulated biogeochemistry in regions where only a specific type of data (e.g. satellite OC, physical variables) is available. The focus on the processes around the spring bloom is a natural choice due to a) the availability of high quality chlorophyll glider data, and b) because the spring bloom is a key driver of the ecosystem dynamics on the NWE Shelf (*Lutz et al.* [2007]; *Henson et al.* [2009]). The results of this study should form a basis for an integrated multi-platform assimilative system, that will optimize the available information from observations and models in order to improve our understanding of the NWE Shelf biogeochemistry. The assimilated biogeochemical glider variables were selected based on the data availability, but both chlorophyll and oxygen are expected to play an important role in the future multi-platform operational assimilation: chlorophyll is a proxy for phytoplankton biomass, which forms the base of the marine food web, while oxygen needs to be monitored and forecast in order to identify oxygen depletion events (i.e. hypoxia, *Vaquer-Sunyer and Duarte* [2008]), which can have disastrous impacts on marine life.

2 Methods

The paper uses a hindcast version of the operational modelling system for the NWE Shelf run by the Met Office in the framework of the CMEMS, i.e. the physical model Nucleus for European Modelling of the Ocean (NEMO, *Madec et al.* [2015]) coupled through the Framework for Aquatic Biogeochemical Models (FABM, *Bruggeman and Bolding* [2014]) with the biogeochemical model European Regional Seas Ecosystem Model (ERSEM, *Baretta et al.* [1995]; *Blackford* [1997]; *Butenschön et al.* [2016]). We used measurements from an AlterEco glider that operated in the central North Sea between May-August 2018 providing data for temperature, salinity, chlorophyll (derived from fluorescence) and oxygen concentrations. In multi-platform assimilation the glider data were complemented with the Ocean Colour-Climate Change Initiative (OC-CCI) satellite product of the European Space Agency (ESA) for total chlorophyll (version 3.1, *Sathyendranath et al.* [2019]), Sea Surface Temperature (SST) data from the GCOM-W1/AMSR-2, NOAA/AVHRR, MetOp/AVHRR, MSG/SEVIRI, Sentinal-3/SLSTR, and Suomi-NPP/VIIRS satellite products, and the temperature and salinity in situ data from the EN4 dataset (*Good et al.* [2013]), which includes profiles from Argo floats, fixed moored arrays, XBTs, CTDs, gliders, and marine mammals. The physical and biogeochemical data were assimilated on a daily basis into NEMO-FABM-ERSEM using NEMOVAR (the assimilative system used operationally by the Met Office, *Mogensen et al.* [2009, 2012]; *Waters et al.* [2015]; *King et al.* [2018]).

The model free simulation was run from 01/09/2017 until the end of the year 2018 and was initialized from a 2016-2018 run of a very similar model configuration presented in *Skákala et al.* [2020]. The free run outputs have been analysed for the period of the glider data availability (08/05-15/08, 2018). The assimilative runs used identical model settings as the free run, only with the added assimilation components. The different as-

similative runs compared in this study are (see also Table 1): a) physical data assimilation (satellite SST, temperature and salinity from EN4 data and the AlterEco glider), b) satellite OC total chlorophyll *a* assimilation, c) AlterEco glider chlorophyll *a* assimilation, d) AlterEco glider oxygen assimilation and e) multi-platform assimilation combining all the data from a)-d). Note that wherever we mention the assimilation of specific data (e.g. glider chlorophyll) we mean a simulation where only those data have been assimilated (as opposed to multi-platform assimilation, which assimilates all the available data). All the assimilative runs were started from the initial value conditions produced by the free simulation for 08/05/2018.

Table 1. The observations assimilated in the different data assimilation (DA) experiments. The table uses some of the following abbreviations: temperature (T), salinity (S) and 'EN4" means the EN4 in situ data-set.

Experiment	satellite SST	EN4 T&S	glider T&S	satellite OC	glider chl *a*	glider O_2
physical DA	Yes	Yes	Yes	No	No	No
satellite OC DA	No	No	No	Yes	No	No
glider chl *a* DA	No	No	No	No	Yes	No
glider O_2 DA	No	No	No	No	No	Yes
Multi-platform DA	Yes	Yes	Yes	Yes	Yes	Yes

2.1 The physical component: NEMO

The NEMO ocean physics component (OPA) is a finite difference, hydrostatic, primitive equation ocean general circulation model (*Madec et al.* [2015]). The NEMO configuration used in this study is similar to the one used by *Ford et al.* [2017]; *Skákala et al.* [2018], and almost identical to *Skákala et al.* [2020]: we use the CO6 NEMO version, based on NEMOv3.6, a development of the CO5 configuration explained in detail by *O'Dea et al.* [2017]. The model has 7 km spatial resolution on the Atlantic Margin Model (AMM7) domain using a terrain-following $z^* - \sigma$ coordinate system with 51 vertical levels (*Siddorn and Furner* [2013]). The lateral boundary conditions for physical variables at the Atlantic boundary were taken from the outputs of the Met Office operational $1/12°$ North Atlantic model (NATL12, *Storkey et al.* [2010]); the Baltic boundary values were derived from a reanalysis produced by the Danish Meteorological Institute for CMEMS. We use annually varying river discharge based on data from *Lenhart et al.* [2010]. The model was forced at the surface by atmospheric fluxes provided by an hourly and 31 km resolution realisation (HRES) of the ERA5 data-set (*https://www.ecmwf.int/*).

2.2 The biogeochemical component: ERSEM

ERSEM (*Baretta et al.* [1995]; *Butenschön et al.* [2016]) is a lower trophic level ecosystem model for marine biogeochemistry, pelagic plankton, and benthic fauna (*Blackford* [1997]). The model splits phytoplankton into four functional types largely based on their size (*Baretta et al.* [1995]): picophytoplankton, nanophytoplankton, diatoms and dinoflagellates. ERSEM uses variable stoichiometry for the simulated plankton groups (*Geider et al.* [1997]; *Baretta-Bekker et al.* [1997]) and each Phytoplankton Functional Type (PFT) biomass is represented in terms of chlorophyll, carbon, nitrogen and phosphorus, with diatoms also represented by silicon. ERSEM predators are composed of three zooplankton types (mesozooplankton, microzooplankton and heterotrophic nanoflagellates), with organic material being decomposed by one functional type of heterotrophic bacteria (*Butenschön et al.* [2016]). The ERSEM inorganic component consists of nutrients (nitrate,

phosphate, silicate, ammonium and carbon) and dissolved oxygen. The carbonate system is also included in the model (*Artioli et al.* [2012]).

We used in this study a similar ERSEM configuration to *Skákala et al.* [2020], but unlike *Skákala et al.* [2020] we implemented an updated ERSEM version (v20.10), with a notable upgrade to the benthic code. The ERSEM parametrization is identical to the one described in *Butenschön et al.* [2016]. The Atlantic boundary values for nitrate, phosphate, silicate and oxygen were taken from World Ocean Atlas (*Garcia et al.* [2013]) and dissolved inorganic carbon from the GLODAP gridded dataset (*Key et al.* [2015]; *Lauvset et al.* [2016]), while plankton and detritus variables were set to have zero fluxes at the Atlantic boundary. The ERSEM irradiance was calculated using a new bio-optical module implemented in the NEMO-FABM-ERSEM AMM7 configuration by *Skákala et al.* [2020]. The bio-optical module resolves light spectrally and distinguishes between downwelling direct and diffuse streams. The module is forced by ERA5 atmospheric inputs (*https://-www.ecmwf.int/*) for total vertically integrated ozone, water vapour, cloud cover, cloud liquid water and sea-level air pressure, as well as by a satellite product for aerosol optical thickness (MODerate resolution Imaging Spectroradiometer, MODIS, *https://modis.-gsfc.nasa.gov/data/dataprod*).

2.3 The assimilative system: NEMOVAR

NEMOVAR is a variational Data Assimilation (DA) system (*Mogensen et al.* [2009, 2012]; *Waters et al.* [2015]) used for operational ocean DA at the Met Office. Via the assimilation of satellite OC derived (total, or PFT) chlorophyll concentrations, NEMOVAR has been demonstrated as being highly successful in improving the phytoplankton community structure (PFT chlorophyll assimilation), phytoplankton seasonal cycle and the timing and magnitude of the spring bloom (*Skákala et al.* [2018, 2020]). There are also indications that satellite OC assimilation can improve the carbon cycle (*Skákala et al.* [2018, 2020]). When it comes to the non-assimilated variables, satellite OC reanalysis typically has a comparable skill to the free run (*Skákala et al.* [2018, 2020]). The satellite OC chlorophyll assimilation using NEMOVAR on the NWE Shelf has been thoroughly validated on bi-decadal time-scales (*Kay et al.* [2019]), showing a good overall skill and no spurious trends in biogeochemical tracer concentrations.

In this study the observations are assimilated on a daily basis. The model is first run for the day and background values are calculated in observation space by interpolating the model fields to the observation locations at the nearest model time step (300 seconds) to the observation time, an approach known as First Guess at Appropriate Time (FGAT). NEMOVAR is then run, calculating a set of increments for each updated variable on the model grid. After the assimilation step the model is re-run with the increments applied to the model variables gradually at each model time-step using incremental analysis updates (IAU, *Bloom et al.* [1996]). For the physical variables the increments are calculated for temperature, salinity, sea surface height and the horizontal velocity components, by accounting for their correlations by transforming those variables through a set of linear balancing equations into an independent set of variables that is assimilated separately. For biogeochemical variables, the increments are initially calculated for the observed variable. For total chlorophyll the assimilation is applied in log-space, since chlorophyll is typically log-normally distributed (*Campbell* [1995]). After calculating the total chlorophyll increments, we use a balancing module to split those increments into the model state variables. The applied scheme (*Skákala et al.* [2018, 2020]) redistributes total chlorophyll increments into the 4 ERSEM PFTs based on background PFT-to-total chlorophyll ratios. The PFT chlorophyll is used to update the remaining PFT components (carbon, phosphorus, nitrogen for all PFTs, silicon for diatoms) following the background stoichiometric ratios. In the case of oxygen assimilation the only updated variable is the simulated oxygen concentration. There were attempts to extend the currently applied balancing scheme to other ERSEM variables (e.g nutrients), but so-far this produced sub-optimal results degrading

the biogeochemical model skill (see discussion in *Skákala et al.* [2018]). Any combined physical-biogeochemical assimilation in NEMOVAR is weakly coupled, which means that the physical and the biogeochemical variables are assimilated separately, with physical assimilation impacting biogeochemistry only through the model dynamics, and no feedback from biogeochemistry to physics.

The multi-platform assimilation is based on the development from *Waters et al.* [2015] extended to biogeochemical variables by *Ford* [2020], i.e. the combined assimilation of satellite OC and glider chlorophyll data is performed by following a scheme previously applied to temperature by *Waters et al.* [2015]. The satellite and in situ glider data are combined to calculate a single set of 3D increments, while allowing for different observation errors to be specified for the different data sources (for the details see *Waters et al.* [2015]; *Ford* [2020]). Since each of the physical data, chlorophyll and oxygen assimilation provides increments for different variables, the multi-platform assimilation simply aggregates the increments from the physical, chlorophyll and oxygen assimilative components.

The background covariances are represented as a product of background variances and a diffusion operator (*Mirouze and Weaver* [2010]; *King et al.* [2018]. Within the diffusion operator, the same length-scales are set for all the assimilated (physical, biogeochemical) variables. The horizontal correlation length-scales are specified a-priori, and are based on two different length scales, a longer 100 km correlation scale and a shorter length-scale based on the first baroclinic Rossby radius of deformation (*King et al.* [2018]). The vertical length-scales use the scheme from *Waters et al.* [2015]; *King et al.* [2018]; *Ford* [2020], where NEMOVAR calculates directly the set of 3D increments (we call this scheme a "3D variant") using flow-dependent vertical length-scales (ℓ), which are the following function of depth (d):

$$\begin{aligned} \ell(d) &= \frac{d_{\mathrm{ml}}}{2} - \left(\frac{1}{2} - \frac{2G(d_{\mathrm{ml}})}{d_{\mathrm{ml}}}\right) \cdot d, \qquad && 0 \le d \le d_{\mathrm{ml}}, \\ \ell(d) &= 2G(d), && d > d_{\mathrm{ml}}, \end{aligned} \tag{1}$$

where d_{ml} is the mixed layer depth (MLD) and $G(d)$ is the vertical grid spacing as a function of depth. Equation 1 means the surface length-scale is equal to half of the MLD, the length scale decreases linearly with depth until the MLD, while beneath MLD the length-scales are two times the local vertical grid resolution. Such vertical correlation length-scales are designed to minimise any spurious mixing of surface increments beneath the mixed layer (*King et al.* [2018]). It should be noted that satellite OC data assimilation in some previous studies (e.g. *Skákala et al.* [2018, 2020]) used a "2D variant", where surface chlorophyll increments were applied throughout the mixed layer. Both 2D and 3D variants were tested in this study and we have found that they produced almost identical results (not shown here). In this study we will present the outputs of the 3D variant, but these are representative of both methods.

NEMOVAR has two important drawbacks: (i) the background errors (square-root of background variances) have to be specified mostly a priori and those do not always capture how the reanalysis approximates the true state, (ii) it does not account for the observational error correlations. Both (i) and (ii) tend to artificially increase the impact of the assimilated observations (especially when there is high density of observations) and likely contribute to the fact that biogeochemical reanalyses on the NWE Shelf are relatively insensitive to the precise value of the background-to-observational error ratio (e.g. *Skákala et al.* [2018]). Then, provided that the reanalysis state is sufficiently internally consistent, NEMOVAR reanalyses on the NWE Shelf tend to converge for a wide interval of background-to-observational error ratios towards the assimilated observations (*Skákala et al.* [2018, 2020]). Improvements could be achieved by using hybrid methods (e.g. background errors calculated as a weighted combination of the parameterised component and a flow-dependent component calculated from an ensemble), or flow-dependent iterative

methods based on error diagnostics, such as the scheme of *Hollingsworth and Lönnberg* [1986]; *Andersson* [2003]; *Desroziers et al.* [2005] (e.g. *Mattern et al.* [2018]; *Cossarini et al.* [2019]). For physical assimilation (*King et al.* [2018]) the background errors were estimated using the innovation method of *Hollingsworth and Lönnberg* [1986] applied to innovations from an existing reanalysis by *O'Dea et al.* [2017], with background errors between 1-3.5 times larger than the observational errors (Table 2). For biogeochemical assimilation the background errors, $\Sigma\{Q_{\mathrm{bkg}}\}$, were estimated from the observational-to-free run differences and observational errors, $\Sigma\{Q_{\mathrm{o}}\}$, (Q_{bkg}, Q_{m} and Q_{o} stand subsequently for the background, model free run and observed concentrations), along the scheme of *Skákala et al.* [2020]:

$$\Sigma\{Q_{\mathrm{bkg}}\} = \sqrt{\langle [Q_{\mathrm{m}} - Q_{\mathrm{o}}]^2 \rangle - \Sigma\{Q_{\mathrm{o}}\}^2}, \tag{2}$$

which assumes that for a suitable spatio-temporal binning the model and observational errors are uncorrelated (*Skákala et al.* [2020]). In the case of the glider data the total observational errors (including representation error) were estimated from the difference between variances of the observations, $V\{Q_{\mathrm{o}}\}$, and the variances of the true state, $V\{Q_{\mathrm{t}}\}$:

$$\Sigma\{Q_{\mathrm{o}}\} = \sqrt{V\{Q_{\mathrm{o}}\} - V\{Q_{\mathrm{t}}\}}, \tag{3}$$

where the variances of the true state were estimated from the model outputs. This scheme assumes that the observations have zero bias and that (for the limited spatio-temporal range of glider data) the observational errors and the true state deviations from the mean are uncorrelated. After estimating the observational errors for gliders, one proceeds with the equation 2 to estimate the corresponding background errors. The methods based on equation 2 and equation 3 produced background and observational errors with comparable values, with background-to-observational error ratios on average between 0.77-2.3 (see Table 2). For the two different chlorophyll observational products, the estimate of glider

Table 2. The Table shows parts of the multi-platform assimilative system with the list of the updated physical-biogeochemical variables and the mean values of the background-to-observational error ratio (B-O error ratio, with error understood as standard deviation). The physical variables are abbreviated as temperature (T), salinity (S), sea surface height (SSH) and horizontal velocity components (U,V).

component	updated variables	B-O error ratio
satellite OC chl *a*	PFT components	2.3
glider chl *a*	PFT components	1.4
glider O_2	oxygen	0.77
satellite T	T,S,SSH,U,V	1.55
in situ T	T,S,SSH,U,V	1.04
in situ S	T,S,SSH,U,V	3.42

chlorophyll error (using equation 3) turned out to be on average 22% lower than the satellite OC chlorophyll error.

2.4 Glider data

The study used data from a Slocum glider (Teledyne Webb Research, Falmouth, USA) named Cabot (Unit 345, National Oceanography Centre, Southampton) deployed during the AlterEco mission (deployment 454). The glider sampling transect was situated in the Central North Sea (see Figure 1), between May-August 2018, collecting data for

temperature and salinity (Seabird SBE42 CTD), colored dissolved organic matter, particulate backscattering, chlorophyll *a* fluorescence (Wetlabs ECOpuck), and oxygen (Aanderaa AA4831 optode). After Quality Control (QC) the quenching-corrected chlorophyll (derived from fluorescence) and oxygen concentrations were available for slightly different periods: chlorophyll for 08/05 - 15/08, 2018 and oxygen for a shorter period of 08/05 - 30/06, 2018. The Cabot glider was chosen because it provided high-quality data, but the period of the glider mission was also of special interest for assimilation, since it marks a known discrepancy between the timing of the spring bloom in the model and observations, with the model biased towards a late bloom (see *Skákala et al.* [2020]). The QC glider outputs contained a substantial number of data-points ($2 \cdot 10^6$ for chlorophyll and $3 \cdot 10^5$ for oxygen) which were mapped to the model AMM7 grid (each observation to the nearest model grid point). The observations that were mapped on the same day into the same model grid point were then averaged into a single value. The grid-averaging of glider observations is a practice adopted in the physical DA to avoid assimilating many observations at higher resolution than the model can represent. However, our tests have shown that the impact of grid-averaging on the biogeochemical reanalysis was negligible. During each day the glider typically covered 3 model horizontal grid-cells and for each model horizontal location the glider scanned nearly the full vertical water column.

The glider data (publicly available from *www.bodc.ac.uk*) were processed by the National Oceanography Centre (NOC) AlterECO team using the GEOMAR glider toolbox for salinity and oxygen lag corrections (following *Bittig et al.* [2014]). The glider was fitted with a standard non-pumped SBE CT sensor, a WETLabs ECOpuck to measure chlorophyll fluorescence, and an Aanderaa 4330 oxygen optode. Oxygen data were corrected based on comparisons between Winkler samples and local crossings with the rest of the AlterEco glider fleet.

The fluorescence sensor on Cabot (454) was calibrated prior to deployment, and recovered data were converted to chlorophyll concentration from raw voltages using the manufacturer supplied calibration routine. The derived chlorophyll record was filtered such that negative values were set to zero. Multiple quenching corrections were tested, including: *Hemsley et al.* [2015]; *Swart et al.* [2015]; *Biermann et al.* [2015] and *Xing et al.* [2012]. The former three methods rely on the use of algal particle scattering to correct for quenching. However, these approaches proved unsatisfactory for use in case-2 waters (e.g. the North Sea). Consequently, the *Xing et al.* [2012] method was adopted. Under this approach the maximum value of chlorophyll concentration above the mixed layer depth (MLD) is extrapolated to the surface for daytime profiles. Night-time chlorophyll profiles are not corrected. MLD is calculated from glider CTD profiles according to the method of *Holte and Talley* [2009].

2.5 Used metrics (definitions)

The paper uses two metrics: a) model-to-observation bias (ΔQ_{mo}) defined as

$$\Delta Q_{\mathrm{mo}} = \langle Q_{\mathrm{m}} - Q_{\mathrm{o}} \rangle, \tag{4}$$

where, as before, Q_{m} are the model free run and Q_{o} the observed concentrations (by the observations we will automatically mean the glider data), and b) Bias-Corrected Root Mean Square Difference (BC RMSD, $\Delta_{\mathrm{RD}} Q_{\mathrm{mo}}$) defined as

$$\Delta_{\mathrm{RD}} Q_{\mathrm{mo}} = \sqrt{\langle [Q_{\mathrm{m}} - Q_{\mathrm{o}} - \Delta Q_{\mathrm{mo}}]^2 \rangle}\ . \tag{5}$$

The BC RMSD metric is applied in two different contexts: as a "spatial BC RMSD" and a "temporal BC RMSD".

In the case of spatial BC RMSD, we calculate for each day (t_{d}) the difference between the model and the observed daily mean, which we call model-to-observation daily bias:

$$\Delta Q_{\mathrm{mo}}(t_d) = \langle Q_{\mathrm{m}}(t_{\mathrm{d}}) - Q_{\mathrm{o}}(t_{\mathrm{d}}) \rangle, \tag{6}$$

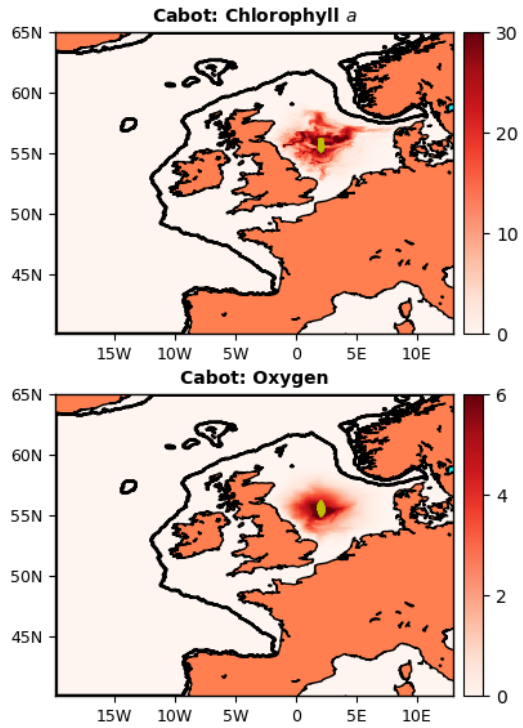

Figure 1. The panels show the NEMO-FABM-ERSEM (AMM7) domain with the Cabot glider data locations (chlorophyll data locations for the full 08/05-15/08, 2018 mission, oxygen data for a shorter period of 08/05-29/06, 2018) marked by yellow dots, as well as glider horizontal area of impact on the reanalysis. The color scale in the two panels shows the weekly (23-29-th June 2018) mean percentage (%) difference between reanalysis and free run in the surface chlorophyll (upper panel) and surface oxygen (bottom panel) concentrations, and reveals the horizontal extent of the glider's impact on the assimilation. The percentage difference is calculated by dividing the absolute value of the difference between reanalysis and the free run, with the free run. The black lines show the boundary of the NWE Shelf (< 200 m bathymetry).

where $Q_{\mathrm{m}}(t_{\mathrm{d}})$ and $Q_{\mathrm{o}}(t_{\mathrm{d}})$ are the model free run and the observation data from the day t_{d}, and the model free run is taken only from the spatial locations visited by the glider (about 150 model grid points per day). Then we calculate "daily BC RMSD", $\Delta_{\mathrm{RD}}Q_{\mathrm{mo}}(t_{\mathrm{d}})$, by applying equation 5 on each day using the model and the observation daily data, as well as their daily biases:

$$\Delta_{\mathrm{RD}}Q_{\mathrm{mo}}(t_{\mathrm{d}}) = \sqrt{\langle [Q_{\mathrm{m}}(t_{\mathrm{d}}) - Q_{\mathrm{o}}(t_{\mathrm{d}}) - \Delta Q_{\mathrm{mo}}(t_{\mathrm{d}})]^2 \rangle}\ . \tag{7}$$

The spatial BC RMSD, $\Delta^{\mathrm{S}}_{\mathrm{RD}}Q_{\mathrm{mo}}$, is then obtained as a time-average of the daily BC RMSD, i.e. averaging $\Delta_{\mathrm{RD}}Q_{\mathrm{mo}}(t_{\mathrm{d}})$ through the glider data availability period (100 days for chlorophyll and 53 days for oxygen):

$$\Delta^{\mathrm{S}}_{\mathrm{RD}}Q_{\mathrm{mo}} = \langle \Delta_{\mathrm{RD}}Q_{\mathrm{mo}}(t_{\mathrm{d}}) \rangle_{t_{\mathrm{d}}}, \tag{8}$$

where $\langle\rangle_{t_{\mathrm{d}}}$ means averaging through the interval of t_{d} values. Since the glider moves on the model grid dominantly in the vertical dimension, the spatial BC RMSD mostly measures how well the model simulation represents the vertical profile of the glider observations.

The temporal BC RMSD, $\Delta^{\mathrm{T}}_{\mathrm{RD}}Q_{\mathrm{mo}}$, is based on calculating a time-series, δ, of the daily mean values (for both model, δ_{m}, and the observations, δ_{o}), averaged through the spatial locations visited by the glider:

$$\delta_{\mathrm{m}}(t_{\mathrm{d}}) = \langle Q(t_{\mathrm{d}}) \rangle, \qquad \delta_{\mathrm{o}}(t_{\mathrm{d}}) = \langle Q_{\mathrm{o}}(t_{\mathrm{d}}) \rangle, \tag{9}$$

then applying equation 5 to those time-series, with bias understood as the model-to-observation difference in the temporal mean of the time-series data:

$$\Delta^{\mathrm{T}}_{\mathrm{RD}}Q_{\mathrm{mo}} = \sqrt{\langle [\delta_{\mathrm{m}}(t_{\mathrm{d}}) - \delta_{\mathrm{o}}(t_{\mathrm{d}}) - \langle \delta_{\mathrm{m}}(t_{\mathrm{d}}) - \delta_{\mathrm{o}}(t_{\mathrm{d}}) \rangle]^2 \rangle_{t_{\mathrm{d}}}}\ . \tag{10}$$

The temporal BC RMSD is designed to capture how the model represents the observed phytoplankton phenology.

It should be noted that the metrics discussed in this section are used to measure "the skill" of the assimilative runs by comparing the simulation outputs to the assimilated glider data, rather than to an independent validation data-set. There are two reasons for this: firstly, to get sufficient validation data for the limited spatio-temporal region of this study is nearly impossible, however, most importantly, this study has no ambition to produce a skill-assessed reanalysis, its ambition is to test the impact of the assimilative system components on the simulated variables. Since the NEMOVAR reanalyses tend to converge under optimal conditions to the assimilated observations (*Skákala et al.* [2018, 2020]), the performance of the assimilative system can be measured by comparing the model to the assimilated data.

3 Results and Discussion

The model free run shows a late and intense spring bloom, with a timing about 1 month later than the bloom observed in the satellite OC and in situ data (Figure 2 and *Skákala et al.* [2020]). The late timing of the model bloom is most likely influenced by the interplay between the model vertical mixing scheme and the simulated irradiance (see the discussion in *Skákala et al.* [2020]). The results from the study of *Skákala et al.* [2020] are confirmed by Figure 3, which shows the chlorophyll concentrations in the region measured by the glider between May and August 2018. When the assimilation starts in early May (Figure 3), the glider is in the post-bloom period showing some deep chlorophyll maxima, whereas the model free run has yet to see the onset of the bloom with chlorophyll concentrations predominantly in the mixed layer. Since the North Atlantic sees substantial seasonal patterns in primary productivity (e.g. *Henson et al.* [2009]), the late and intense model bloom has a large impact on the biogeochemical model skill (*Skákala et al.* [2020]).

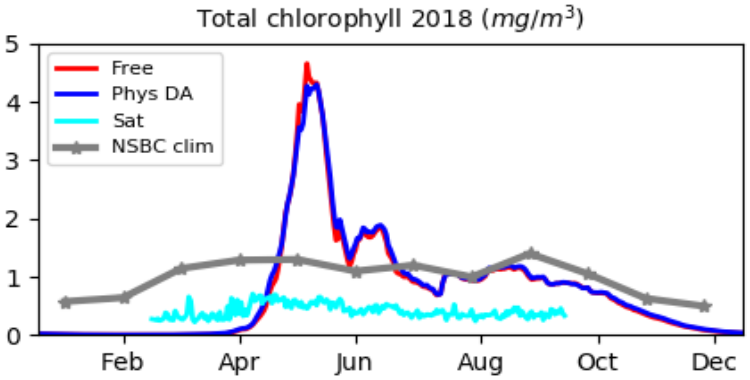

Figure 2. The mean daily surface chlorophyll concentrations averaged across the NWE Shelf for the year 2018. We compare a model free run used in this study with the physical data assimilation (the physical data assimilation started on 01/09 2017 from the model free run initial values), the satellite OC and the North Sea Biogeochemical Climatology (NSBC) in situ data set (*Hinrichs et al.* [2017]). The satellite OC chlorophyll values are masked for the October-February period when there is sparsity of data due to the extensive cloud cover and the low solar zenith angle. The model is shown to have an intense and late spring bloom: the observed bloom is much less pronounced than the bloom in the model and the timing of the observed bloom is around the early April, as opposed to the early-mid May bloom simulated by the model.

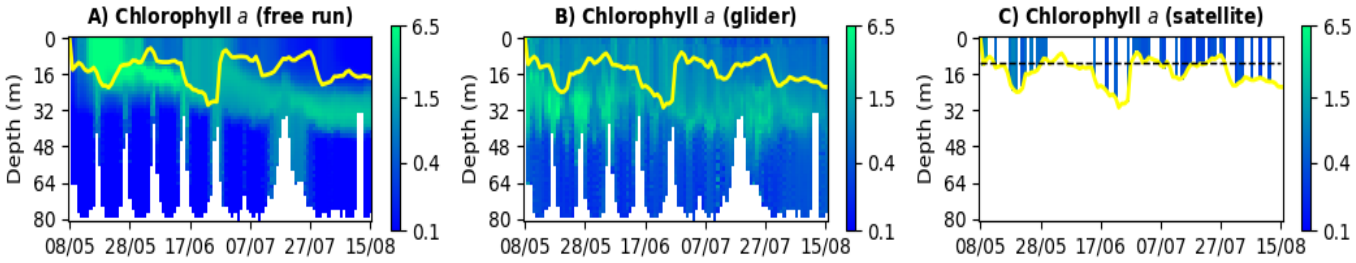

Figure 3. Hovmöller diagrams for the model free run and the observations. The left panel (A) shows the model free run outputs for total chlorophyll *a* (mg m^{-3}) horizontally averaged through the area covered by the glider during each day (the plot is depth vs time). The middle panel (B) shows the same for the glider-observed chlorophyll concentrations and the right panel (C) shows the satellite OC chlorophyll observations at the glider locations. The yellow lines mark the mixed layer depth of the model free run (left-hand panel) and of the physics-assimilative run (the middle and right-hand panels). The satellite observations are plotted in the mixed layer, with the dotted black line broadly corresponding to the average satellite optical depth (*Skákala et al.* [2020]). The several missing data in the right hand plot are due to the cloud cover. The missing data at the bottom of panels A-B are due to the varying bathymetry along the horizontal glider trajectory.

The simulated surface chlorophyll on the NWE Shelf is typically corrected by the assimilation of OC satellite data (*Skákala et al.* [2018, 2020]) and the positive impact of satellite OC assimilation on the simulated NWE Shelf surface chlorophyll is shown in Figure 4:A-B. Around the glider locations, it is shown that both satellite OC and glider chlorophyll assimilation remove the late simulated bloom and improve the surface phytoplankton phenology (Figure 5:D,F, Figure 6:A-B). However, unlike the satellite OC component, the glider chlorophyll assimilation has a limited impact on the model domain (Figure 4:D). The horizontal spatial impact of glider assimilation varies with time (Figure 7A-B), but any substantial impact of glider assimilation on the simulated chlorophyll (on the level of >10%) is typically constrained to a 50 km radius around the glider location (Figure 7:A).

Since glider chlorophyll *a* data were assimilated across the whole water column, the glider chlorophyll assimilation is also able to substantially improve the sub-surface chlorophyll concentrations (Figure 5:F). The three skill metrics (bias, spatial and temporal BC RMSD) capturing how the simulated chlorophyll *a* matches with the glider observations were all substantially improved by the glider chlorophyll assimilation: the model bias was reduced by almost 50% (Table 3 and Figure 6:D), the spatial BC RMSD by 60% (Table 3) and the temporal BC RMSD by 70% (Table 3). Unlike glider chlorophyll assimilation, satellite OC assimilation updates chlorophyll concentrations only in the mixed layer, but the model dynamics propagates the updates to chlorophyll beneath the mixed layer and gradually spreads the impact of assimilation across the whole water column (Figure 5:C). It is encouraging to see that the model dynamics acting on the satellite OC assimilation increments produces a qualitatively similar change to the sub-surface chlorophyll as the glider assimilation (Figure 5:C and Figure 5:E). We propose a simple explanation based on chlorophyll dynamics: The satellite-only assimilative run removes the intense late model bloom in May, removing chlorophyll from the mixed layer and increasing the light penetrating into the water column. The increased irradiance combined with nutrient availability produces deep chlorophyll maxima around the pycnocline (Figure 5:C). Furthermore, the removal of the late (mid-May) bloom in the satellite OC reanalysis means the assimilation also removes the gradually deepening chlorophyll maxima (the July-August period in Figure 3:B and Figure 4:C), as the nutrients become confined deeper in the water column. The satellite OC assimilation improves both temporal BC RMSD (by 55%, Table 3) and spatial BC RMSD (by 15%, Table 3). Although the improvement of BC RMSD is in both cases outperformed by the glider chlorophyll assimilation, the substantial reduction of temporal BC RMSD by 55% in the satellite OC reanalysis is non-trivial, and it is only possible due to (i) a relative consistency between the satellite OC data and the glider surface measurements (Figure 3, Figure 6:A-B), and (ii) a realistic update to sub-surface chlorophyll driven by the model dynamics.

Whilst the physical data assimilation improves the model representation of both temperature and salinity (Figure 6), it is unable to correct the late model spring bloom (Figure 2) and has a relatively modest impact on chlorophyll concentrations (Figure 3:C, Figure 5:C,E, Figure 8:E). This can be understood as follows: As the pycnocline is primarily controlled by temperature and salinity, we expect that assimilating the physical variables may improve vertical gradients in water density and consequently vertical mixing. However, in the well-mixed nutrient-rich waters the onset of the spring bloom depends on the interplay between vertical mixing in the upper oceanic layer and the irradiance (e.g. *Huisman et al.* [1999]; *Waniek* [2003]; *Smyth et al.* [2014]). Such interplay is closely related to the model atmospheric forcing product for the wind stress and the net incoming short-wave radiation, but an even greater issue is the model response to the used atmospheric forcing product, which consists here mostly of the ERSEM underwater light attenuation, the phytoplankton response to specific light conditions and the model vertical mixing scheme. The ERSEM response to the atmospheric forcing is known to be sensitive to the forcing temporal resolution, leading to shifts of up to one week in the timing of the phytoplankton bloom (*Powley et al.* [2020]). Since the assimilation does not alter the atmospheric forc-

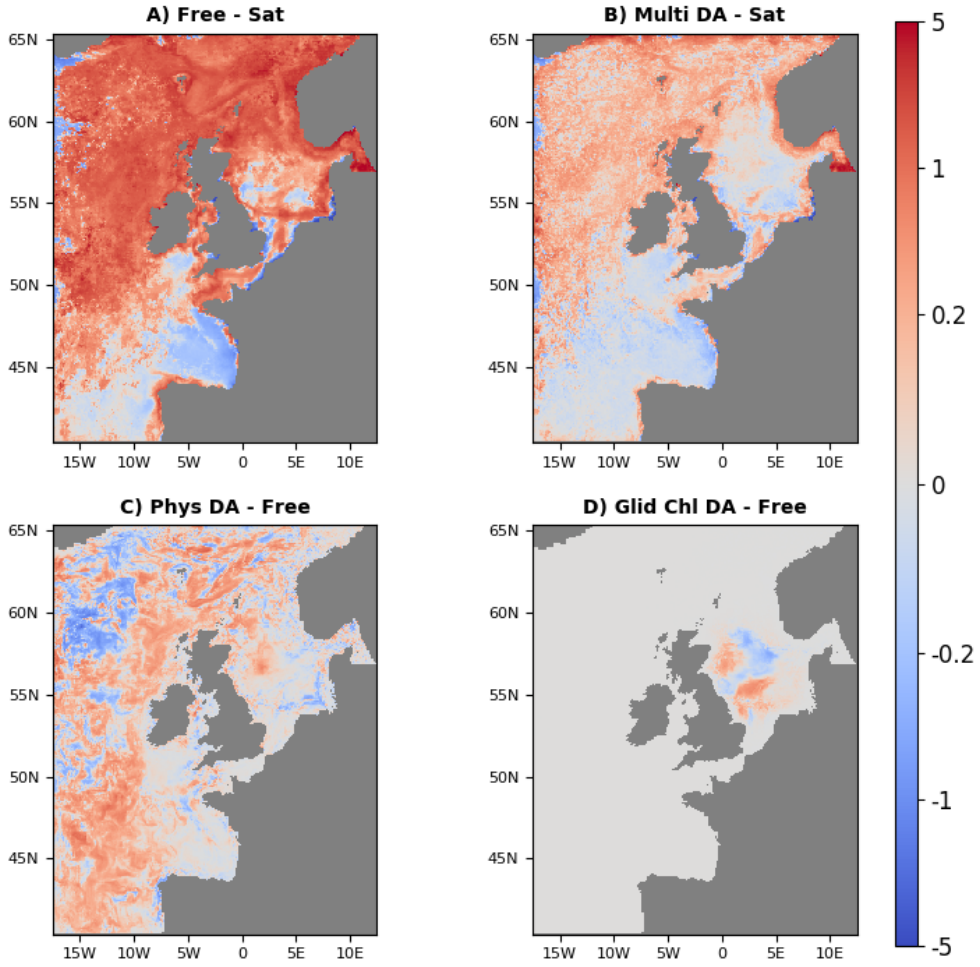

Figure 4. Comparison of the time median surface chlorophyll *a* distributions (mg m^{-3}) for the simulation period (08/05 - 15/08, 2018) and the AMM7 domain. The upper two panels show differences in the mean concentrations between the free run (panel A), the multi-platform reanalysis (panel B) and the assimilated satellite OC product (the differences are simulated minus observed chlorophyll). The bottom two panels display the impact of the physical (panel C) and the glider chlorophyll (panel D) assimilation on the simulated surface chlorophyll *a* concentrations by showing the differences between the two reanalyses and the free run (reanalysis minus free run). The NWE Shelf-wide impact of the multi-platform assimilation on the surface chlorophyll *a* concentrations is dominated by the satellite OC assimilation component (not shown here). The multi-platform reanalysis (panel B) is therefore almost identical to satellite OC reanalysis.

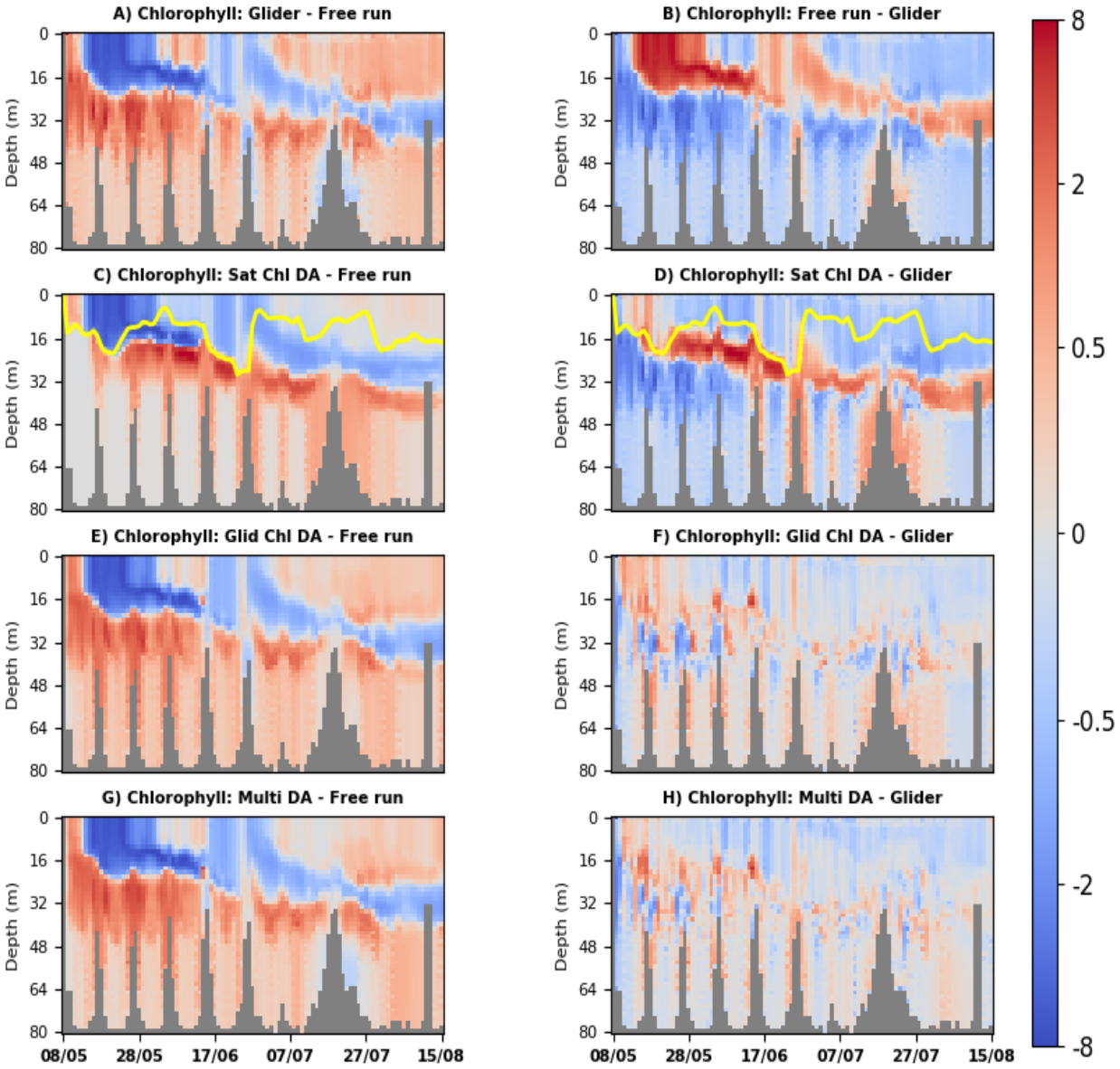

Figure 5. The left hand panels (A,C,E,G) demonstrate the spatio-temporal impact of the multi-platform system components on the simulated chlorophyll *a* concentrations (mg m^{-3}) by comparing different simulations to the free run. One major advantage of the left-hand side panels is that they demonstrate how the changes introduced by the assimilation propagate vertically with the model dynamics, e.g. for the satellite OC assimilation (panel C) that updates the model only in the mixed layer (the MLD is marked in panels C-D by a yellow line). The right hand panels (B,D,F,H) show the skill of each component by comparing the simulations to the glider observations. The first row shows the skill of the free run (panel B) and the required changes to the free run in order to better match the glider observations (panel A). The rows beneath the first row compare the chosen reference (free run or glider) with a range of system components: i) the reanalysis assimilating satellite OC chlorophyll (panels C and D), ii) the reanalysis assimilating glider chlorophyll (panels E and F) and iii) the multi-platform assimilation (joint physical data, glider chlorophyll and oxygen, and satellite chlorophyll assimilation, panels G and H).

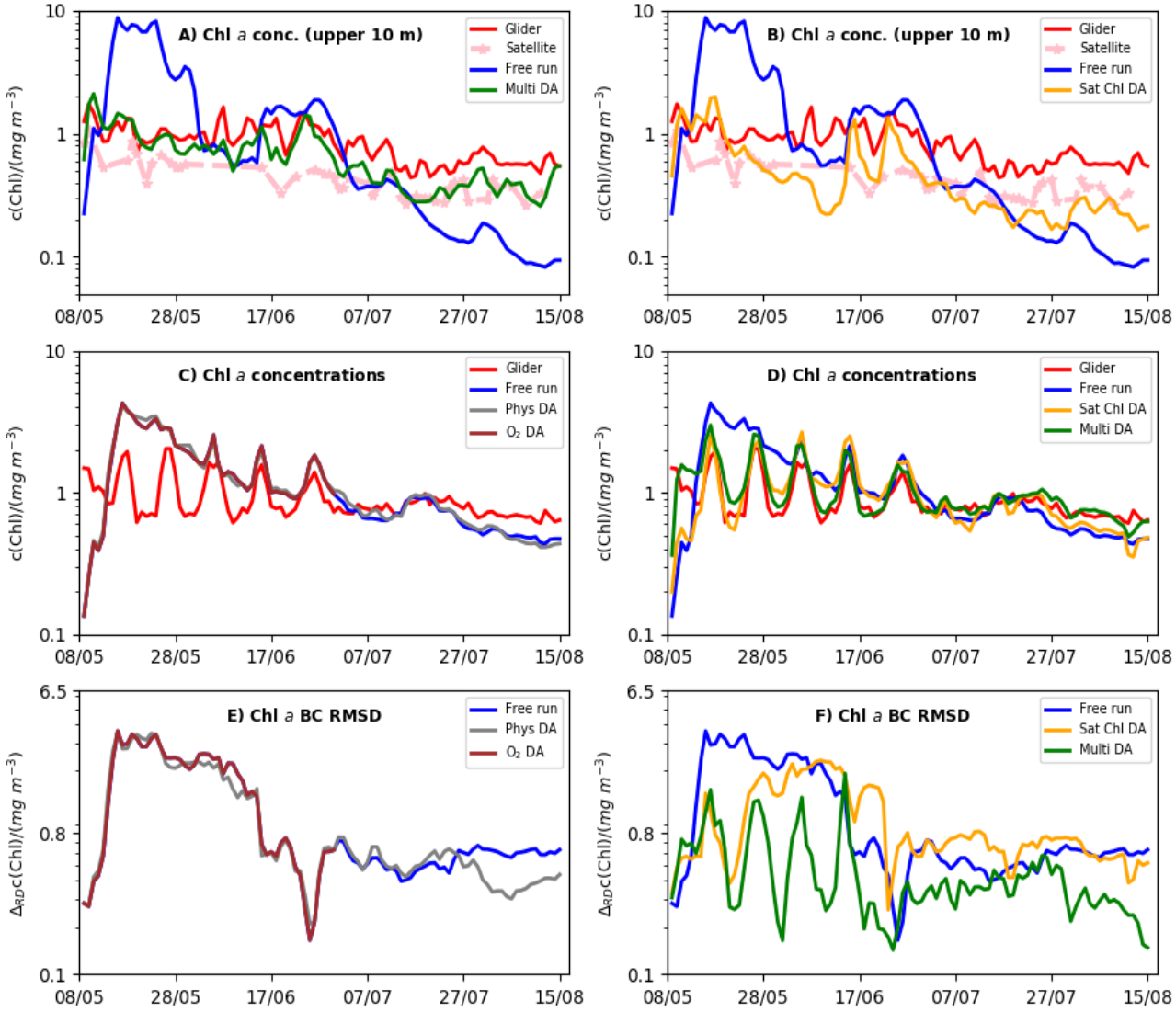

Figure 6. The impact of different multi-platform system components on the model chlorophyll concentrations. The panels A-B compare the daily chlorophyll values spatially averaged throughout the upper 10 meters of the water column, within the part of the model domain visited by the glider. The panels C-D show the daily values spatially averaged throughout the whole water column, within the part of the model domain visited by the glider (the daily time series from equation 9), and the remaining panels E-F show the daily BC RMSD (equation 7) for the same part of the model domain as the panels C-D. The panels display the skill of the following system components: physical data assimilation (grey color), satellite OC chlorophyll assimilation (orange) and oxygen assimilation (brown). These components are compared with the multi-platform assimilative run (joint physical data, glider chlorophyll and oxygen, and satellite OC chlorophyll assimilation, green color), the free run (blue), the glider observations (red) and the satellite OC data (pink).

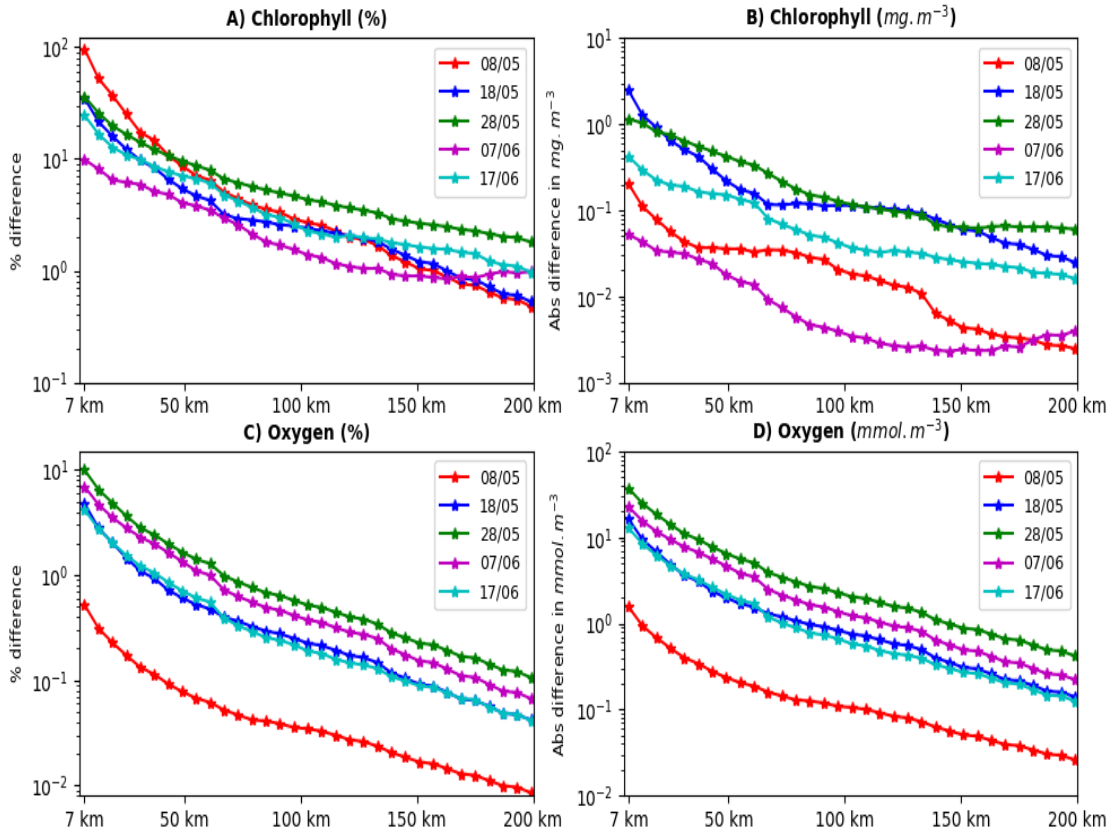

Figure 7. The horizontal scales for the impact of the glider chlorophyll (panels A-B) and the glider oxygen (panels C-D) assimilation. The impact of glider assimilation is shown for a range of days (between 08/05-17/06, 2018). The impact is calculated by comparing the mean absolute value of the difference in chlorophyll (A-B panels), or oxygen (panels C-D) concentration between the reanalysis and the model free run. The mean absolute difference is shown relative to the free run values (in %, panels A,C), or in the absolute values (panels B,D). The absolute difference was averaged on the circles with 7-200 km radii (the spatial scales shown on the x-axis). The circles were centered around the glider daily mean location. The mean absolute differences (y-axis) are shown on a log-scale, a straight-line therefore represents an exponential decrease of the assimilation impact as a function of spatial scale.

Table 3. The Table demonstrates the skill measured by bias (equation 4), spatial BC RMSD (equation 8) and temporal BC RMSD (equation 10) of the free run and the relative (%) changes to the skill carried by the different assimilative system components. The skill compares the model simulations with the glider data. The percentage changes in the columns for the assimilative runs are calculated relative to the free run skill. The negative percentage means that the bias, or (spatial, temporal) BC RMSD is reduced by the specific system component, whilst the positive percentages mean that bias, or (spatial, temporal) BC RMSD, increases.

variable	free run	phys DA	sat Chl *a* DA	glid Chl *a* DA	O_2 DA	multi DA
Chl *a* bias	0.31 mg m^{-3}	+6.8%	-80%	-46.4%	0%	-56.7%
Chl *a* temporal BC RMSD	0.77 mg m^{-3}	+5.2%	-54.6%	-70.3%	0%	-65.4%
Chl *a* spatial BC RMSD	1.14 mg m^{-3}	-5.5%	-15.3%	-61.9%	0%	-59%
O_2 bias	25 mmol m^{-3}	-3.8%	+10.6%	+0.7%	-97%	-98%
O_2 temporal BC RMSD	13.5 mmol m^{-3}	-4.3%	+10.8%	-5.4%	-83.8%	-83.7%
O_2 spatial BC RMSD	29.8 mmol m^{-3}	-7%	-5.7%	-14.6%	-44.5%	-47.4%

ing, the model mixing scheme, or the phytoplankton response to light, assimilating physical data was found to have relatively modest impact on chlorophyll bias, as well as spatial and temporal BC RMSD (between 5-7%, Table 3). However, the impact of physical data assimilation on the simulated phytoplankton could become more substantial within a strongly coupled system (*Goodliff et al.* [2019]). In such system we would mutually update the biogeochemical and the physical increments within a balancing scheme, which could be ideally defined using a two-way coupled physical-biogeochemical model (e.g. *Lengaigne et al.* [2007]). Such development is planned in the foreseeable future.

Finally, we have observed that assimilating glider oxygen into the model has a negligible impact on the simulated chlorophyll concentrations, with a change to the skill metrics of the order $O(10^{-2})$ percent (Table 3, see also Figure 5:C,E). This is expected, as within ERSEM the oxygen variable influences phytoplankton concentrations only indirectly through a complex chain of marine chemical and biological processes (e.g. through influencing remineralization, or nitrification rates, and through the impact of hypoxia on zooplankton).

There is a clear discrepancy between the oxygen time series of the glider and the model free run (Figure 9, Figure 10:A-B), with glider oxygen concentrations steadily decreasing, while the simulated oxygen peaks in late May (Figure 10:A-B). Furthermore, simulated oxygen concentrations have a substantial positive bias (25 mmol m^{-3}, Table 3, Figure 10:A-B) relative to the glider observations. Figure 9:A clearly shows that photosynthesis is an important driver of the simulated oxygen, producing a large oxygen surge in the mixed layer during the simulated late spring bloom. Some connection between oxygen and chlorophyll concentrations (a proxy for primary productivity) appears also in the glider observations (Figure 9:B), with the peak in oxygen concentrations located in the neighborhood of the glider deep chlorophyll maxima (Figure 3:B). As for chlorophyll, a simple way to improve simulated oxygen is to assimilate the glider oxygen data into the model (Figure 10:D, Figure 11:H). Assimilating glider oxygen into the model reduces the oxygen bias by 97%, temporal BC RMSD by 84% and spatial BC RMSD by 45% (Table 3). However, as in the case of chlorophyll, such assimilation has a limited spatial impact on the NWE Shelf (Figure 7:C-D and Figure 12:C). Unlike chlorophyll, the glider oxygen assimilation horizontal impact reduces with spatial scale at a rate largely independent of

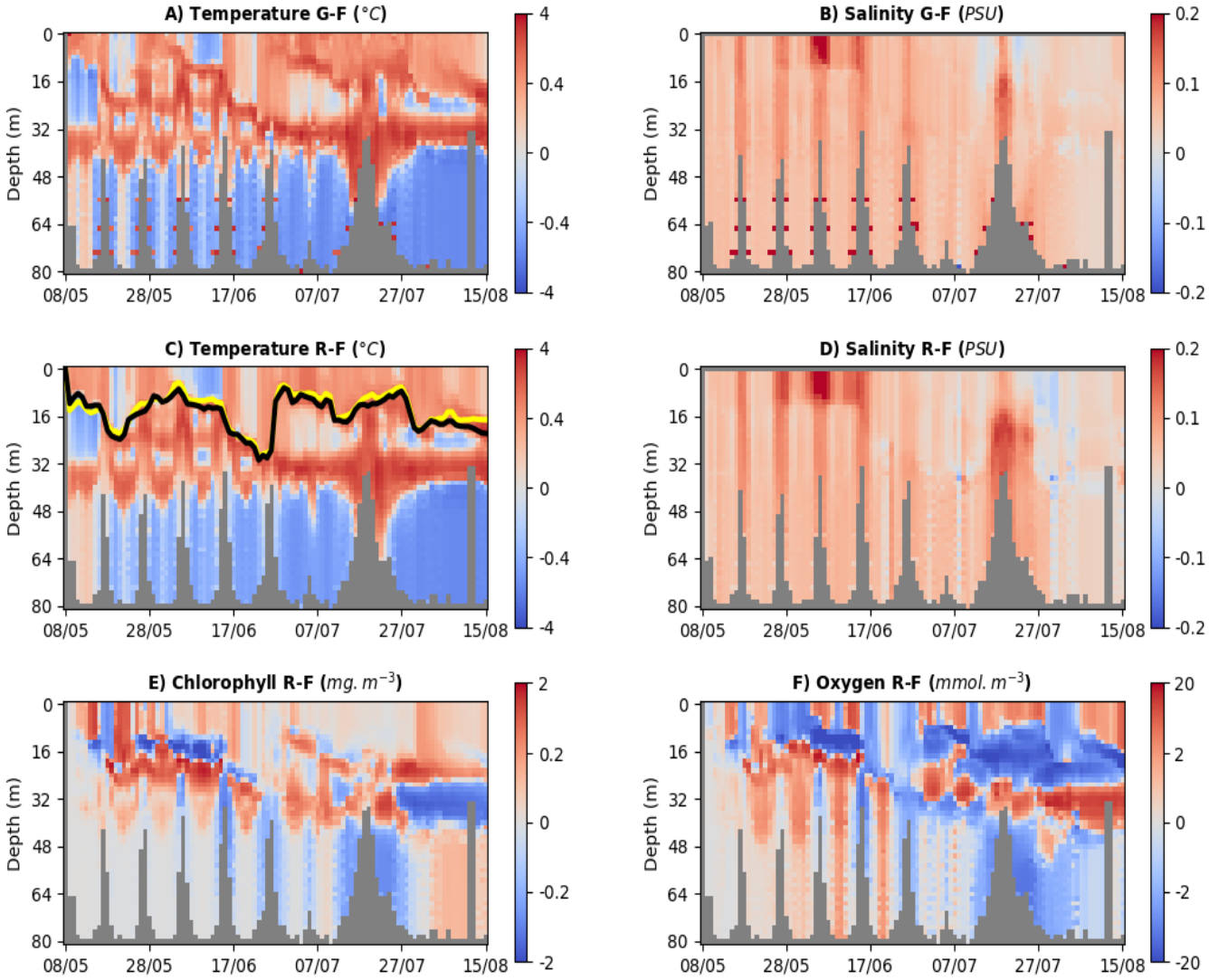

Figure 8. Hovmöller diagrams to demonstrate the impact of physical (SST, in situ temperature and salinity, including Cabot glider data) assimilation on the model variables. The upper row (A and B) shows the difference between glider ("G" in the title) and free run ("F") outputs for temperature (A) and salinity (B). The middle row (C and D) shows differences for the same variables between physical reanalysis ("R") and the free run. The bottom row (E and F) shows the same differences between physical reanalysis and the free run, but for the two biogeochemical variables addressed by this study: total chlorophyll and oxygen. The two lines in the panel C compare the mixed layer depth of the free run (yellow) and of the physical reanalysis (black). The mixed layer depth has been obtained in both cases from the model outputs.

time (Figure 7:C-D). Beyond the 50 km scale the assimilation horizontal impact decays approximately exponentially (a straight line in Figure 7:C-D), with a halving scale of approximately 40 km, which means the impact is reduced by an order of magnitude at a 130 km scale.

Since the modeled oxygen concentrations are largely driven by the phytoplankton seasonal cycle, it is not surprising that assimilation of either satellite OC, or glider chlorophyll, has a major influence on the simulated oxygen (Figure 11:C,E, Figure 12:B). The assimilated chlorophyll modifies the simulated oxygen after a necessary time-lag, removing the excess oxygen from the model spring bloom and generating some deep oxygen maxima in early-to-mid June (Figure 11:C-F). The chlorophyll assimilation consistently improves oxygen in the period up to the start of June, but typically degrades oxygen in early-to-mid June (Figure 10:B,D,F), mostly due to the surge in oxygen concentrations around the deep oxygen maxima (Figure 11:C,E). The oxygen surge is likely to be partly driven by the deep chlorophyll maxima, e.g. by the overestimated chlorophyll concentrations around the deep maxima in the satellite OC assimilation (Figure 5:D). However, other drivers such as zooplankton and bacteria respiration are likely to contribute to the deep oxygen maxima. The mechanism for this is suggested by Figure 13:C-F: the chlorophyll assimilation removes phytoplankton biomass from the mixed layer, limiting the resources for the simulated zooplankton and bacteria, and reducing their concentrations. The reduced phytoplankton concentrations seem to have much larger and more consistent impact on the zooplankton concentrations than on bacteria (Figure 13:C-F) and the reduced zooplankton concentration means less oxygen is removed through respiration, which likely produces excess oxygen concentrations.

Compared to chlorophyll assimilation, the physical data assimilation has a relatively modest impact on the simulated oxygen (Figure 8:F, Figure 12:A-B), but it tends to consistently improve both the oxygen bias, and the spatial and temporal BC RMSD (by $3-7\%$, Table 3). The impact of physical data assimilation on the oxygen concentrations can be explained by the lowered oxygen saturation concentrations under the increase in temperature within the reanalysis (Figure 8:C).

Finally, we have combined all the assimilative system components (physical data assimilation, satellite OC, glider chlorophyll and oxygen) into a multi-platform assimilative run and we have shown that multi-platform assimilation has the capability to optimally combine the skill of all its components (Figure 4:B, Figure 6:D,F, Figure 9:D-E, Table 3). The multi-platform chlorophyll re-analysis is dominated in the vicinity of the glider by the glider chlorophyll assimilative component (Figure 5:E,G), whilst further away from the glider it is dominated by the satellite OC assimilation (Figure 4:D). The multi-platform oxygen re-analysis is dominated near the glider locations by the glider oxygen assimilation (Figure 10:D), whilst further away from the glider locations it is dominantly shaped by the satellite OC assimilation (Figure 12:B,D).

4 Summary

Present and future glider missions on the NWE Shelf will provide us with three-dimensional (3D) data on some specific biogeochemical variables (presently mostly for chlorophyll and oxygen) combined with physical measurements (e.g. temperature and salinity). These data will be, together with satellite missions, integrated into our ecosystem models by means of a multi-platform assimilative system. It is of crucial importance to understand what observed variables need to be assimilated in order to represent well a target ecosystem indicator, and what assimilation may need to be avoided because it can paradoxically degrade the model skill for the target indicator. Furthermore, different data will be available for different spatial and temporal regions on the NWE Shelf and it is essential to understand how the limitations imposed by the availability of the observational data impact on the quality of the multi-platform reanalyses. To address these questions we

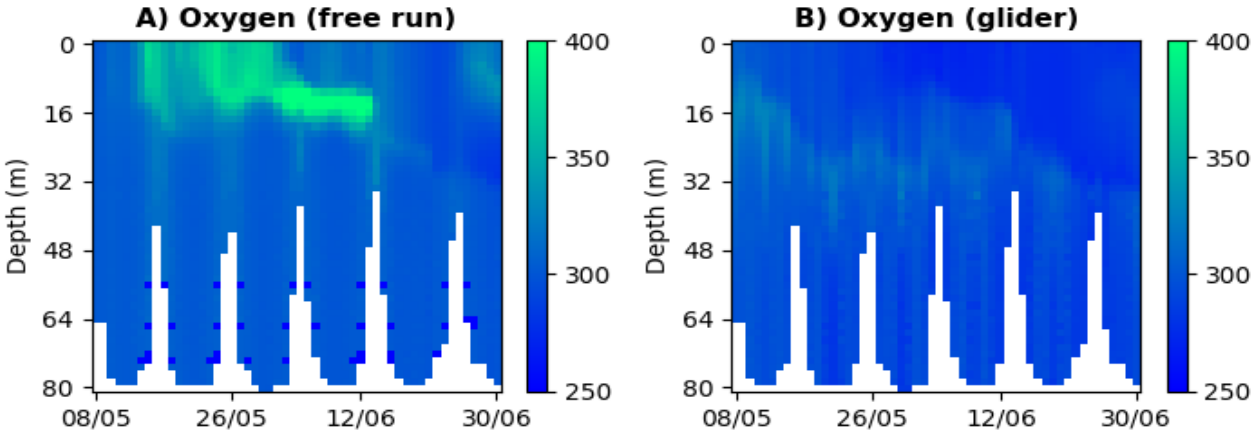

Figure 9. Hovmöller diagrams for the model free run and the glider observations. The left-hand panel (A) shows the model free run outputs for oxygen (mmol m^{-3}) horizontally averaged through the area covered by the glider during each day (the plot is depth vs time). The right-hand panel (B) shows the same for the glider-observed oxygen.

explored the impact of different system components (physical data, satellite OC chlorophyll, glider chlorophyll and oxygen assimilation) on the simulated ecosystem state, using the operational set-up currently assimilating physical variables and satellite OC chlorophyll. This study has taught us several important lessons:

a) Assimilating physical data (SST, in situ temperature and salinity) has a negligible impact on the simulated phytoplankton bloom. This is because the modeled phytoplankton bloom depends in the North Sea mostly on the model response to the atmospheric forcing (wind stress and solar radiance), which remains unchanged by the temperature and salinity assimilation. Since the phytoplankton bloom is an essential driver of the ecosystem dynamics on the NWE Shelf (*Henson et al.* [2009]), it is quite likely that physical glider data assimilation has a relatively minor importance for the simulated ecosystem dynamics on the NWE Shelf. This is quite different from some other global regions where physical assimilation is either desirable (*Anderson et al.* [2000]; *Yu et al.* [2018]), or can degrade the biogeochemical model skill (*Berline et al.* [2007]; *Holt et al.* [2014]; *Raghukumar et al.* [2015]; *Park et al.* [2018]). Based on this study we would suggest that, at least around the spring bloom in the North Sea, physical assimilation can be used to improve the physical model skill, whilst its impact on the coupled biogeochemical model can be relatively ignored.

b) In terms of chlorophyll, the glider chlorophyll assimilation is the dominant and best performing component of the multi-platform assimilative system within the 50 km horizontal proximity of the glider. Further away from the glider locations, assimilating satellite OC data substantially improves the surface chlorophyll concentrations, but it can also produce realistic updates to the sub-surface chlorophyll. Since satellite OC assimilation updates chlorophyll only within the mixed layer, the updates to the sub-surface chlorophyll are explained by the model dynamical response to the assimilation. The skill of satellite OC assimilation in sub-surface chlorophyll is important, as glider technology will be able to cover only limited parts of the NWE Shelf and future multi-platform assimilative system will have to rely heavily on satellite data.

c) The modelled phytoplankton dynamics is impacted by the oxygen concentrations only indirectly, e.g. through remineralization, or nitrification rates and the impact of hy-

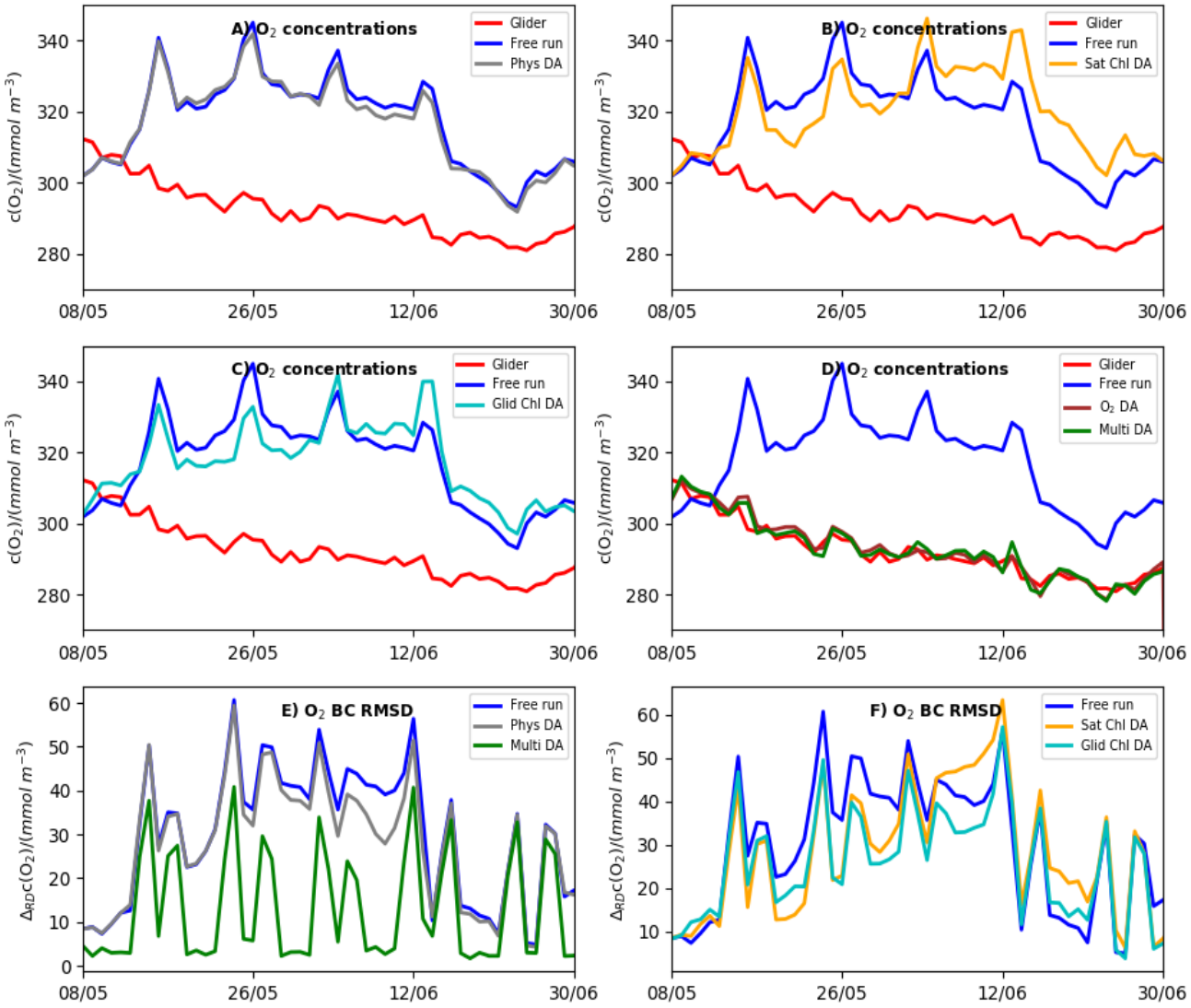

Figure 10. The impact of different multi-platform system components on the model oxygen. The panels A-D compare the daily oxygen values spatially averaged throughout the whole water column, within the part of the model domain visited by the glider (the daily time series from equation 9), and the panels E-F show the daily BC RMSD (equation 7). The panels display the skill of the following system components: physical data assimilation (grey color), satellite OC chlorophyll assimilation (orange), glider chlorophyll assimilation (light blue) and oxygen assimilation (brown). These components are compared with the multi-platform assimilative run (joint physical data, glider chlorophyll and oxygen, and satellite chlorophyll assimilation, green color), the free run (blue) and the glider observations (red).

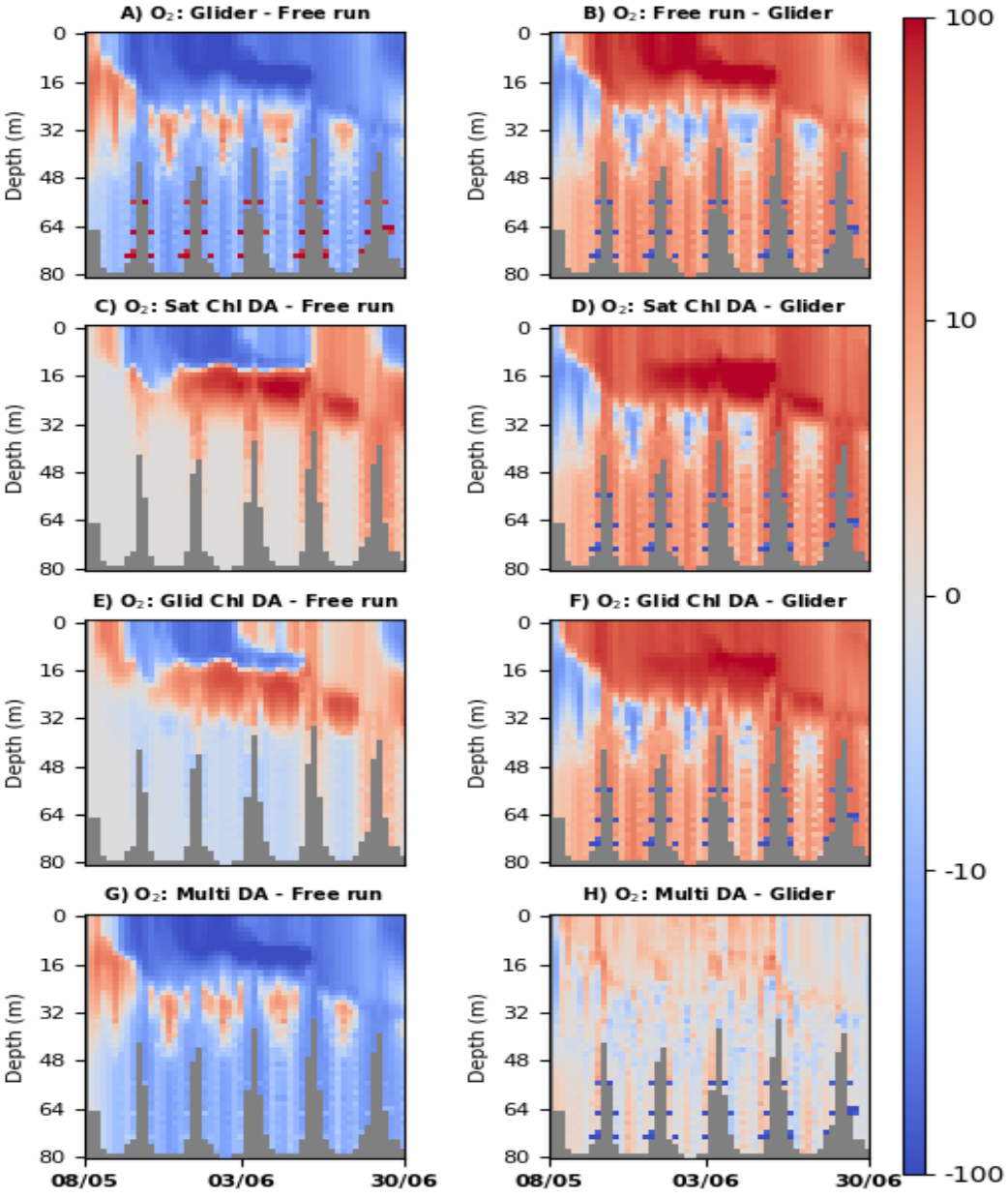

651 **Figure 11.** The left hand panels (A,C,E,G) demonstrate the impact of the multi-platform system compo-
652 nents on the simulated oxygen concentrations (mmol m^{-3}) by comparing different simulations to the free
653 run. These panels are particularly well suited to see how chlorophyll assimilation dynamically influences
654 the simulated oxygen. The right hand panels (B,D,F,H) show the skill of each component by comparing the
655 simulations to the glider observations. The first row shows the skill of the free run (panel B) and the required
656 changes to the free run in order to better match the glider observations (panel A). The rows beneath the first
657 row compare the chosen reference (free run or glider) with a range of system components: i) the reanalysis
658 assimilating satellite OC chlorophyll (panels C and D), ii) the reanalysis assimilating glider chlorophyll (pan-
659 els E and F) and iii) the multi-platform assimilation (joint physical data, glider chlorophyll and oxygen, and
660 satellite chlorophyll assimilation, panels G and H).

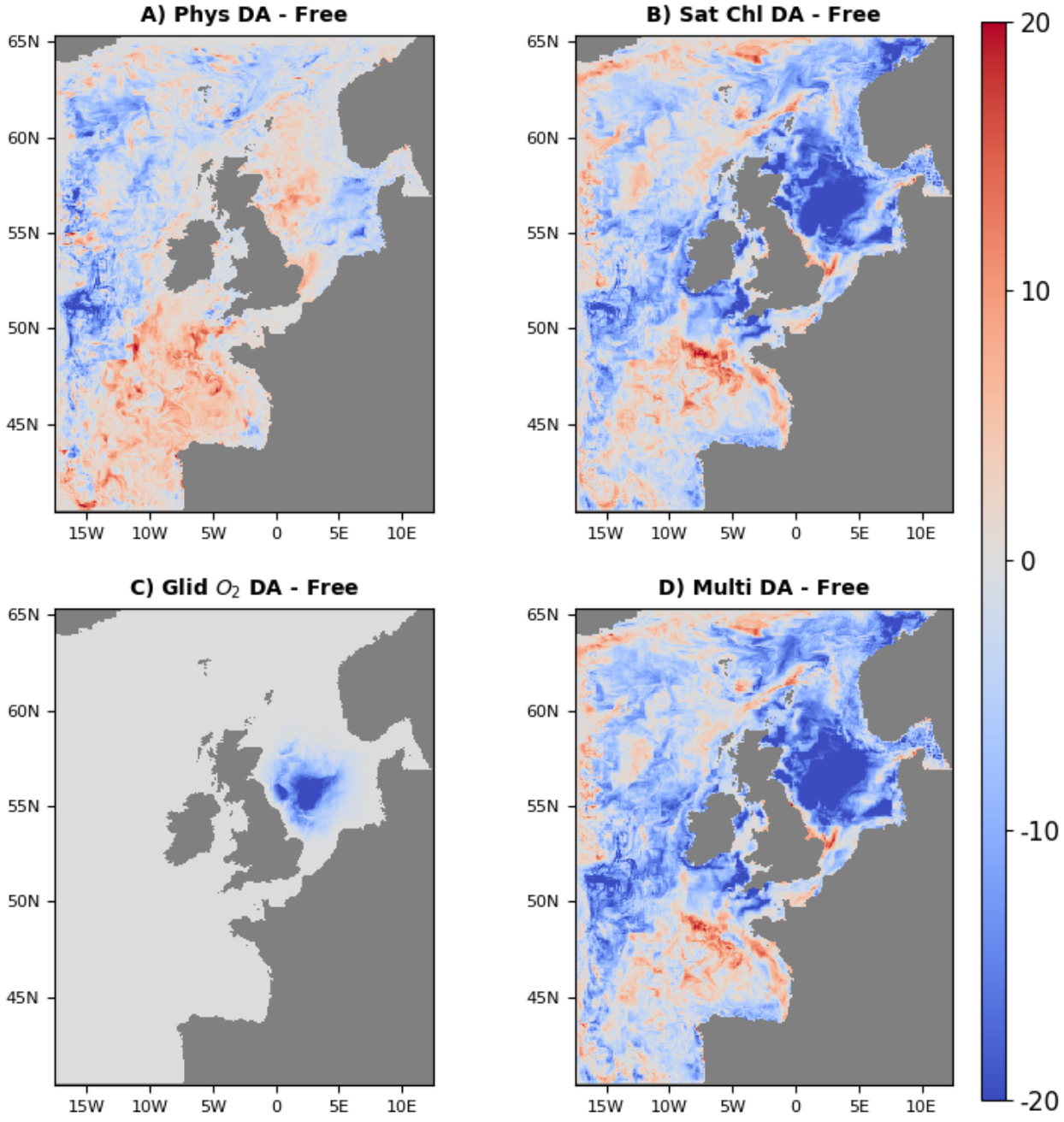

Figure 12. Comparison of the time median surface oxygen distributions (mmol m^{-3}) for the oxygen glider data period (08/05/2018 - 29/06, 2018). The panels show the impact of the different multi-platform system components on the modelled oxygen by comparing the differences between four reanalyses and the free run. The reanalyses presented in the panels are the physical data assimilation (panel A), the OC satellite chlorophyll assimilation (panel B), the glider oxygen assimilation (panel C) and the multi-platform assimilation (panel D).

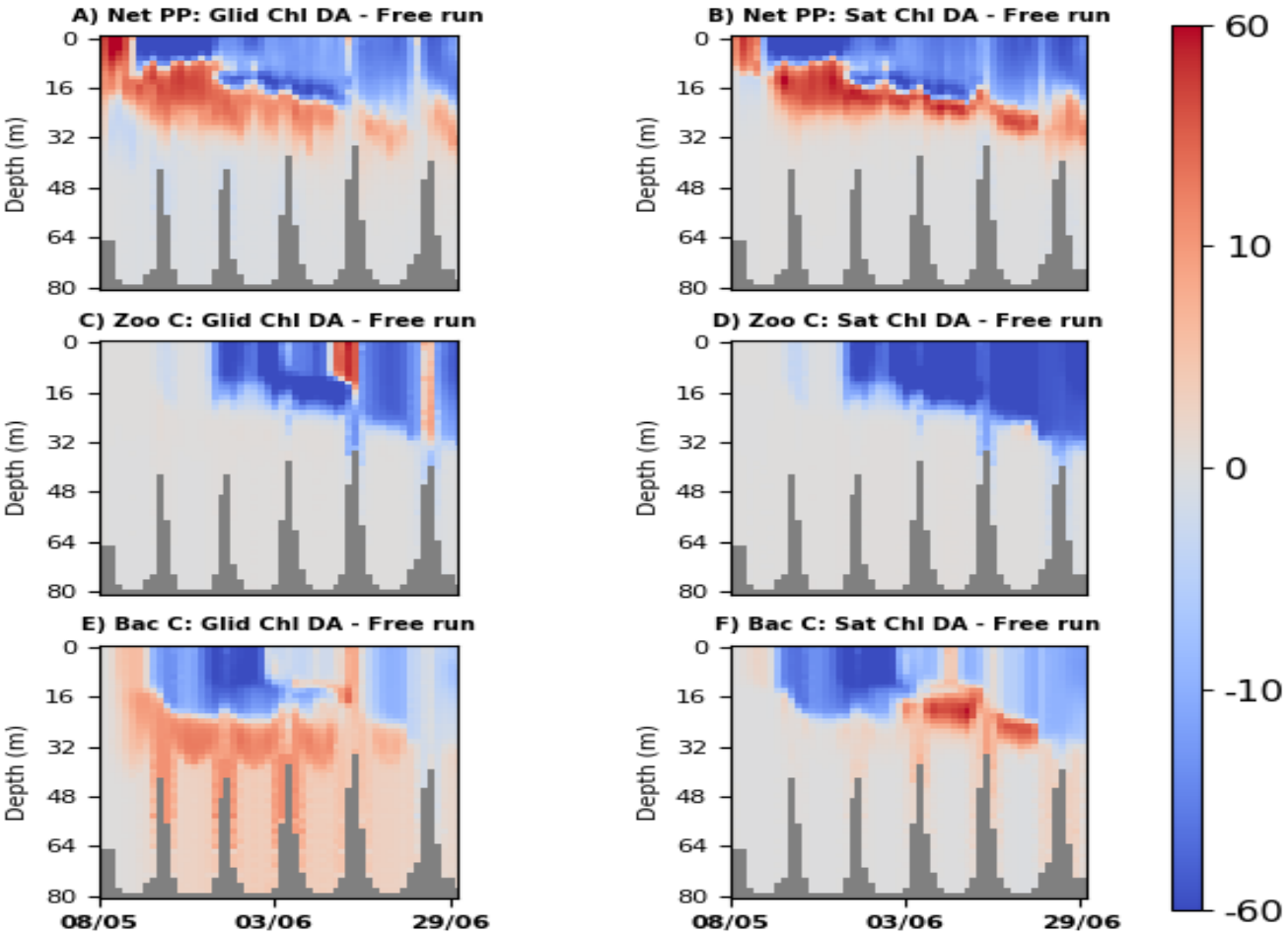

Figure 13. The different panels help to interpret the impact of the simulated primary production and respiration on the modeled oxygen concentrations. We show the difference between the glider chlorophyll assimilation (left-hand side panels, A,C,E), or OC chlorophyll assimilation (right-hand side panels, B,D,F) and the model free run (always assimilative run minus free run). The difference is shown for (i) the total net primary production (mg C $m^{-3}day^{-1}$, panels A-B), (ii) total zooplankton carbon concentrations (mg C m^{-3}, panels C-D) and (iii) heterotrophic bacteria carbon concentrations (mg C m^{-3}, panels E-F).

poxia on zooplankton (*Butenschön et al.* [2016]). It is therefore hardly surprising that univariate assimilation of oxygen has a negligible impact on the simulated phytoplankton chlorophyll concentrations. This also means that one can assimilate oxygen into ERSEM without worrying about its consequences for the modelled phytoplankton. Such an oxygen assimilation has an obvious advantage in that it outperforms any other run in the model simulation of oxygen.

d) Two important drivers of the simulated oxygen concentrations are the primary production and respiration. Consequently, assimilating (satellite OC, or glider) chlorophyll was found to have a major impact on the modeled oxygen. The removal of the late model bloom in the reanalysis improves the modeled oxygen, however it produces spurious deep oxygen maxima, partly due to the productivity at the deep chlorophyll maxima and partly due to the reduced respiration by the ERSEM zooplankton. Physical data assimilation has a stronger impact on the oxygen than on chlorophyll (oxygen saturation levels depend substantially on temperature), but it had substantially less impact on the simulated oxygen than the chlorophyll assimilation.

e) The multi-platform assimilation (joint physical data, glider chlorophyll and oxygen, satellite OC chlorophyll assimilation) combines optimally the skill of its components and always performs comparably to, or better than its best performing component.

f) Based on the results of this study we expect that the multi-platform system will provide us with improved-quality operational products on the NWE Shelf.

Acknowledgments

This work was supported by a joint effort of Natural Environment Research Council (NERC) funded projects of the Marine Integrated Autonomous Observing Systems (MIAOS) programme: Combining Autonomous observations and Models for Predicting and Understanding Shelf seas (CAMPUS) and Alternative Framework to Assess Marine Ecosystem Functioning in Shelf Seas (AlterECO, *http://projects.noc.ac.uk/altereco/*), grant no. NE/P013899/1. The work also benefited from the Copernicus Marine Environment Monitoring Service (CMEMS) funded projects OPTIcal data Modelling and Assimilation (OPTIMA) and NOWMAPS. The work contributes to the SEAMLESS project, which received funding from the European Union's Horizon 2020 research and innovation programme under grant agreement no. 101004032. This work was also supported by the UK National Centre for Earth Observation (NCEO). The European Regional Seas Ecosyetem Model (ERSEM) code v20.10 can be publicly traced on *https://doi.org/10.5281/zenodo.4075315* and the Framework for Aquatic Biogeochemical Models (FABM) v1.0 on *https://doi.org/10.5281/zenodo.4075315*. We thank the European Space Agency Climate Initiative "Ocean Color" (*https://esa-oceancolour-cci.org/*) for providing the ocean color data. The glider data used in the study (doi:10.5285/b57d215e-065f-7f81-e053-6c86abc01a82) are publicly available on *https://www.bodc.ac.uk/data/published_data_library/catalogue/*. The model was forced by atmospheric ERA5 product of The European Centre for Medium-Range Weather Forecasts (ECMWF, *https://www.ecmwf.int/*). The river forcing data used by the model were prepared by Sonja van Leeuwen and Helen Powley as part of UK Shelf Seas Biogeochemistry programme (contract no. NE/K001876/1) of the NERC and the Department for Environment Food and Rural Affairs (DEFRA). We acknowledge use of the MONSooN system, a collaborative facility supplied under the Joint Weather and Climate Research Programme, a strategic partnership between the Met Office and the NERC. The different outputs for the free run simulations and reanalyses are stored on the MONSooN storage facility MASS and can be obtained upon request.

References

Allen, J., M. Eknes, and G. Evensen (2003), An ensemble kalman filter with a complex marine ecosystem model: hindcasting phytoplankton in the cretan sea, in *Annales Geophysicae*, vol. 21, pp. 399–411.

Anderson, L. A., A. R. Robinson, and C. J. Lozano (2000), Physical and biological modeling in the gulf stream region:: I. data assimilation methodology, *Deep Sea Research Part I: Oceanographic Research Papers*, *47*(10), 1787–1827.

Andersson, E. (2003), Modelling the temporal evolution of innovation statistics, *This volume*, pp. 153–164.

Artioli, Y., J. C. Blackford, M. Butenschön, J. T. Holt, S. L. Wakelin, H. Thomas, A. V. Borges, and J. I. Allen (2012), The carbonate system in the north sea: Sensitivity and model validation, *Journal of Marine Systems*, *102*, 1–13.

Baretta, J., W. Ebenhöh, and P. Ruardij (1995), The european regional seas ecosystem model, a complex marine ecosystem model, *Netherlands Journal of Sea Research*, *33*(3-4), 233–246.

Baretta-Bekker, J., J. Baretta, and W. Ebenhöh (1997), Microbial dynamics in the marine ecosystem model ersem ii with decoupled carbon assimilation and nutrient uptake, *Journal of Sea Research*, *38*(3-4), 195–211.

Bell, M. J., A. Schiller, P.-Y. Le Traon, N. Smith, E. Dombrowsky, and K. Wilmer-Becker (2015), An introduction to godae oceanview.

Berline, L., J.-M. Brankart, P. Brasseur, Y. Ourmières, and J. Verron (2007), Improving the physics of a coupled physical–biogeochemical model of the north atlantic through data assimilation: Impact on the ecosystem, *Journal of Marine Systems*, *64*(1-4), 153–172.

Biermann, L., C. Guinet, M. N. Bester, A. Brierley, and L. Boehme (2015), An alternative method for correcting fluorescence quenching.

Bittig, H. C., B. Fiedler, R. Scholz, G. Krahmann, and A. Körtzinger (2014), Time response of oxygen optodes on profiling platforms and its dependence on flow speed and temperature, *Limnology and Oceanography: Methods*, *12*(8), 617–636.

Blackford, J. (1997), An analysis of benthic biological dynamics in a north sea ecosystem model, *Journal of Sea Research*, *38*(3-4), 213–230.

Bloom, S., L. Takacs, A. Da Silva, and D. Ledvina (1996), Data assimilation using incremental analysis updates, *Monthly Weather Review*, *124*(6), 1256–1271.

Borges, A., L.-S. Schiettecatte, G. Abril, B. Delille, and F. Gazeau (2006), Carbon dioxide in european coastal waters, *Estuarine, Coastal and Shelf Science*, *70*(3), 375–387.

Bruggeman, J., and K. Bolding (2014), A general framework for aquatic biogeochemical models, *Environmental modelling & software*, *61*, 249–265.

Butenschön, M., J. Clark, J. N. Aldridge, J. I. Allen, Y. Artioli, J. Blackford, J. Bruggeman, P. Cazenave, S. Ciavatta, S. Kay, et al. (2016), Ersem 15.06: a generic model for marine biogeochemistry and the ecosystem dynamics of the lower trophic levels, *Geoscientific Model Development*, *9*(4), 1293–1339.

Campbell, J. W. (1995), The lognormal distribution as a model for bio-optical variability in the sea, *Journal of Geophysical Research: Oceans*, *100*(C7), 13,237–13,254.

Carmillet, V., J.-M. Brankart, P. Brasseur, H. Drange, G. Evensen, and J. Verron (2001), A singular evolutive extended kalman filter to assimilate ocean color data in a coupled physical–biochemical model of the north atlantic ocean, *Ocean Modelling*, *3*(3-4), 167–192.

Ciavatta, S., R. Torres, S. Saux-Picart, and J. I. Allen (2011), Can ocean color assimilation improve biogeochemical hindcasts in shelf seas?, *Journal of Geophysical Research: Oceans*, *116*(C12).

Ciavatta, S., R. Torres, V. Martinez-Vicente, T. Smyth, G. Dall'Olmo, L. Polimene, and J. I. Allen (2014), Assimilation of remotely-sensed optical properties to improve marine biogeochemistry modelling, *Progress in oceanography*, *127*, 74–95.

Ciavatta, S., S. Kay, S. Saux-Picart, M. Butenschön, and J. Allen (2016), Decadal reanalysis of biogeochemical indicators and fluxes in the north west european shelf-sea ecosystem, *Journal of Geophysical Research: Oceans*, *121*(3), 1824–1845.

Ciavatta, S., R. Brewin, J. Skakala, L. Polimene, L. de Mora, Y. Artioli, and J. I. Allen (2018), Assimilation of ocean-color plankton functional types to improve marine ecosystem simulations, *Journal of Geophysical Research: Oceans*, *123*(2), 834–854.

Ciavatta, S., S. Kay, R. Brewin, R. Cox, A. Di Cicco, F. Nencioli, L. Polimene, M. Sammartino, R. Santoleri, J. Skákala, et al. (2019), Ecoregions in the mediterranean sea through the reanalysis of phytoplankton functional types and carbon fluxes, *Journal of Geophysical Research: Oceans*.

Cossarini, G., P. Lermusiaux, and C. Solidoro (2009), Lagoon of venice ecosystem: Seasonal dynamics and environmental guidance with uncertainty analyses and error subspace data assimilation, *Journal of Geophysical Research: Oceans*, *114*(C6).

Cossarini, G., L. Mariotti, L. Feudale, A. Mignot, S. Salon, V. Taillandier, A. Teruzzi, and F. D'Ortenzio (2019), Towards operational 3d-var assimilation of chlorophyll biogeochemical-argo float data into a biogeochemical model of the mediterranean sea, *Ocean Modelling*, *133*, 112–128.

Desroziers, G., L. Berre, B. Chapnik, and P. Poli (2005), Diagnosis of observation, background and analysis-error statistics in observation space, *Quarterly Journal of the Royal Meteorological Society: A journal of the atmospheric sciences, applied meteorology and physical oceanography*, *131*(613), 3385–3396.

Doney, S. C. (1999), Major challenges confronting marine biogeochemical modeling, *Global Biogeochemical Cycles*, *13*(3), 705–714.

Doney, S. C., K. Lindsay, K. Caldeira, J.-M. Campin, H. Drange, J.-C. Dutay, M. Follows, Y. Gao, A. Gnanadesikan, N. Gruber, et al. (2004), Evaluating global ocean carbon models: The importance of realistic physics, *Global Biogeochemical Cycles*, *18*(3).

El Moussaoui, A., C. Perruche, E. Greiner, C. Ethé, and M. Gehlen (2011), Integration of biogeochemistry into mercator ocean systems, *Mercator Océan Newsletter*, *40*, 3–14.

Fontana, C., C. Grenz, and C. Pinazo (2010), Sequential assimilation of a year-long time-series of seawifs chlorophyll data into a 3d biogeochemical model on the french mediterranean coast, *Continental Shelf Research*, *30*(16), 1761–1771.

Ford, D. (2020), Assimilating synthetic biogeochemical-argo and ocean colour observations into a global ocean model to inform observing system design, *submitted to Biogeosciences, freely available at https://www.biogeosciences-discuss.net/bg-2020-152/bg-2020-152.pdf*.

Ford, D., and R. Barciela (2017), Global marine biogeochemical reanalyses assimilating two different sets of merged ocean colour products, *Remote Sensing of Environment*, *203*, 40–54.

Ford, D., K. Edwards, D. Lea, R. Barciela, M. Martin, and J. Demaria (2012), Assimilating globcolour ocean colour data into a pre-operational physical-biogeochemical model, *Ocean Science*, *8*(5), 751–771.

Ford, D. A., J. van der Molen, K. Hyder, J. Bacon, R. Barciela, V. Creach, R. McEwan, P. Ruardij, and R. Forster (2017), Observing and modelling phytoplankton community structure in the north sea, *Biogeosciences*, *14*(6), 1419–1444.

Friedlingstein, P., P. Cox, R. Betts, L. Bopp, W. von Bloh, V. Brovkin, P. Cadule, S. Doney, M. Eby, I. Fung, et al. (2006), Climate–carbon cycle feedback analysis: results from the c4mip model intercomparison, *Journal of climate*, *19*(14), 3337–3353.

Garcia, H. E., R. A. Locarnini, T. P. Boyer, J. I. Antonov, O. K. Baranova, M. M. Zweng, J. R. Reagan, D. R. Johnson, A. V. Mishonov, and S. Levitus (2013), World ocean atlas 2013. volume 4, dissolved inorganic nutrients (phosphate, nitrate, silicate).

Geider, R., H. MacIntyre, and T. Kana (1997), Dynamic model of phytoplankton growth and acclimation: responses of the balanced growth rate and the chlorophyll a: carbon ratio to light, nutrient-limitation and temperature, *Marine Ecology Progress Series*, *148*, 187–200.

Germineaud, C., J.-M. Brankart, and P. Brasseur (2019), An ensemble-based probabilistic score approach to compare observation scenarios: an application to biogeochemical-argo deployments, *Journal of Atmospheric and Oceanic Technology*, (2019).

Good, S. A., M. J. Martin, and N. A. Rayner (2013), En4: Quality controlled ocean temperature and salinity profiles and monthly objective analyses with uncertainty estimates, *Journal of Geophysical Research: Oceans*, *118*(12), 6704–6716.

Goodliff, M., T. Bruening, F. Schwichtenberg, X. Li, A. Lindenthal, I. Lorkowski, and L. Nerger (2019), Temperature assimilation into a coastal ocean-biogeochemical model: assessment of weakly and strongly coupled data assimilation, *Ocean Dynamics*, *69*(10), 1217–1237.

Gregg, W. W. (2008), Assimilation of seawifs ocean chlorophyll data into a three-dimensional global ocean model, *Journal of Marine Systems*, *69*(3-4), 205–225.

Gregg, W. W., and C. S. Rousseaux (2017), Simulating pace global ocean radiances, *Frontiers in Marine Science*, *4*, 60.

Hemsley, V. S., T. J. Smyth, A. P. Martin, E. Frajka-Williams, A. F. Thompson, G. Damerell, and S. C. Painter (2015), Estimating oceanic primary production using vertical irradiance and chlorophyll profiles from ocean gliders in the north atlantic, *Environmental science & technology*, *49*(19), 11,612–11,621.

Henson, S. A., J. P. Dunne, and J. L. Sarmiento (2009), Decadal variability in north atlantic phytoplankton blooms, *Journal of Geophysical Research: Oceans*, *114*(C4).

Hinrichs, I., V. Gouretski, J. Pätch, K. Emeis, and D. Stammer (2017), North sea biogeochemical climatology.

Hollingsworth, A., and P. Lönnberg (1986), The statistical structure of short-range forecast errors as determined from radiosonde data. part i: The wind field, *Tellus A*, *38*(2), 111–136.

Holt, J., J. I. Allen, T. R. Anderson, R. Brewin, M. Butenschön, J. Harle, G. Huse, P. Lehodey, C. Lindemann, L. Memery, et al. (2014), Challenges in integrative approaches to modelling the marine ecosystems of the north atlantic: Physics to fish and coasts to ocean, *Progress in Oceanography*, *129*, 285–313.

Holte, J., and L. Talley (2009), A new algorithm for finding mixed layer depths with applications to argo data and subantarctic mode water formation, *Journal of Atmospheric and Oceanic Technology*, *26*(9), 1920–1939.

Hoteit, I., G. Triantafyllou, G. Petihakis, and J. Allen (2003), A singular evolutive extended kalman filter to assimilate real in situ data in a 1-d marine ecosystem model.

Hoteit, I., G. Triantafyllou, and G. Petihakis (2005), Efficient data assimilation into a complex, 3-d physical-biogeochemical model using partially-local kalman filters.

Huisman, J., P. van Oostveen, and F. J. Weissing (1999), Critical depth and critical turbulence: two different mechanisms for the development of phytoplankton blooms, *Limnology and oceanography*, *44*(7), 1781–1787.

Ishizaka, J. (1990), Coupling of coastal zone color scanner data to a physical-biological model of the southeastern us continental shelf ecosystem: 2. an eulerian model, *Journal of Geophysical Research: Oceans*, *95*(C11), 20,183–20,199.

Jahnke, R. A. (2010), Global synthesis, in *Carbon and nutrient fluxes in continental margins*, pp. 597–615, Springer.

Johnson, K. (2016), The scientific rationale, design and implementation plan for a biogeochemical-argo float array, *Planning Group Rep.*

Johnson, K., and H. Claustre (2016), Bringing biogeochemistry into the argo age, *Eos*, *97*(10.1029).

Jones, E. M., M. E. Baird, M. Mongin, J. Parslow, J. Skerratt, J. Lovell, N. Margvelashvili, R. J. Matear, K. Wild-Allen, B. Robson, et al. (2016), Use of remote-sensing reflectance to constrain a data assimilating marine biogeochemical model of the great barrier reef, *Biogeosciences*, *13*(23), 6441–6469.

Kalaroni, S., K. Tsiaras, G. Petihakis, I. Hoteit, A. Economou-Amilli, and G. Triantafyllou (2016), Data assimilation of depth-distributed satellite chlorophyll-α in two mediter-

ranean contrasting sites, *Journal of Marine Systems*, *160*, 40–53.

Kay, S., R. McEwan, and D. Ford (2019), North west european shelf production centre northwestshelf_analysis_forecast_bio_004_011, quality information document, *Copernicus Marine Environment Monitoring Service*.

Key, R. M., A. Olsen, S. van Heuven, S. K. Lauvset, A. Velo, X. Lin, C. Schirnick, A. Kozyr, T. Tanhua, M. Hoppema, et al. (2015), Global ocean data analysis project, version 2 (glodapv2).

King, R. R., J. While, M. J. Martin, D. J. Lea, B. Lemieux-Dudon, J. Waters, and E. O'Dea (2018), Improving the initialisation of the met office operational shelf-seas model, *Ocean Modelling*, *130*, 1–14.

Lauvset, S. K., R. M. Key, A. Olsen, S. van Heuven, A. Velo, X. Lin, C. Schirnick, A. Kozyr, T. Tanhua, M. Hoppema, et al. (2016), A new global interior ocean mapped climatology: The 1× 1 glodap version 2, *Earth System Science Data*, *8*, 325–340.

Legge, O., M. Johnson, N. Hicks, T. Jickells, M. Diesing, J. Aldridge, J. Andrews, Y. Artioli, D. C. Bakker, M. T. Burrows, et al. (2020), Carbon on the northwest european shelf: Contemporary budget and future influences, *Frontiers in Marine Science*, *7*, 143.

Lellouche, J.-M., O. Le Galloudec, M. Drévillon, C. Régnier, E. Greiner, G. Garric, N. Ferry, C. Desportes, C.-E. Testut, C. Bricaud, et al. (2013), Evaluation of global monitoring and forecasting systems at mercator océan, *Ocean Science*, *9*(1), 57.

Lenartz, F., C. Raick, K. Soetaert, and M. Grégoire (2007), Application of an ensemble kalman filter to a 1-d coupled hydrodynamic-ecosystem model of the ligurian sea, *Journal of Marine Systems*, *68*(3-4), 327–348.

Lengaigne, M., C. Menkes, O. Aumont, T. Gorgues, L. Bopp, J.-M. André, and G. Madec (2007), Influence of the oceanic biology on the tropical pacific climate in a coupled general circulation model, *Climate Dynamics*, *28*(5), 503–516.

Lenhart, H.-J., D. K. Mills, H. Baretta-Bekker, S. M. Van Leeuwen, J. Van Der Molen, J. W. Baretta, M. Blaas, X. Desmit, W. Kühn, G. Lacroix, et al. (2010), Predicting the consequences of nutrient reduction on the eutrophication status of the north sea, *Journal of Marine Systems*, *81*(1-2), 148–170.

Lutz, M. J., K. Caldeira, R. B. Dunbar, and M. J. Behrenfeld (2007), Seasonal rhythms of net primary production and particulate organic carbon flux to depth describe the efficiency of biological pump in the global ocean, *Journal of Geophysical Research: Oceans*, *112*(C10).

Madec, G., et al. (2015), Nemo ocean engine.

Mattern, J. P., C. A. Edwards, and A. M. Moore (2018), Improving variational data assimilation through background and observation error adjustments, *Monthly Weather Review*, *146*(2), 485–501.

Mirouze, I., and A. Weaver (2010), Representation of correlation functions in variational assimilation using an implicit diffusion operator, *Quarterly Journal of the Royal Meteorological Society*, *136*(651), 1421–1443.

Mogensen, K., M. Balmaseda, A. Weaver, M. Martin, and A. Vidard (2009), Nemovar: A variational data assimilation system for the nemo ocean model, *ECMWF newsletter*, *120*, 17–22.

Mogensen, K., M. A. Balmaseda, A. Weaver, et al. (2012), The nemovar ocean data assimilation system as implemented in the ecmwf ocean analysis for system 4.

Natvik, L.-J., and G. Evensen (2003), Assimilation of ocean colour data into a biochemical model of the north atlantic: Part 1. data assimilation experiments, *Journal of Marine Systems*, *40*, 127–153.

Nerger, L., and W. W. Gregg (2007), Assimilation of seawifs data into a global ocean-biogeochemical model using a local seik filter, *Journal of Marine Systems*, *68*(1-2), 237–254.

Nerger, L., and W. W. Gregg (2008), Improving assimilation of seawifs data by the application of bias correction with a local seik filter, *Journal of marine systems*, *73*(1-2), 87–102.

O'Dea, E., R. Furner, S. Wakelin, J. Siddorn, J. While, P. Sykes, R. King, J. Holt, and H. Hewitt (2017), The co5 configuration of the 7 km atlantic margin model: large-scale biases and sensitivity to forcing, physics options and vertical resolution, *Geoscientific Model Development*, *10*(8), 2947.

Oschlies, A., and V. Garçon (1999), An eddy-permitting coupled physical-biological model of the north atlantic: 1. sensitivity to advection numerics and mixed layer physics, *Global Biogeochemical Cycles*, *13*(1), 135–160.

Park, J.-Y., C. A. Stock, X. Yang, J. P. Dunne, A. Rosati, J. John, and S. Zhang (2018), Modeling global ocean biogeochemistry with physical data assimilation: a pragmatic solution to the equatorial instability, *Journal of Advances in Modeling Earth Systems*, *10*(3), 891–906.

Pauly, D., V. Christensen, S. Guénette, T. J. Pitcher, U. R. Sumaila, C. J. Walters, R. Watson, and D. Zeller (2002), Towards sustainability in world fisheries, *Nature*, *418*(6898), 689.

Powley, H. R., J. Bruggeman, J. Hopkins, T. Smyth, and J. Blackford (2020), Sensitivity of shelf sea marine ecosystems to temporal resolution of meteorological forcing, *Journal of Geophysical Research: Oceans*, p. e2019JC015922.

Pradhan, H. K., C. Völker, S. Losa, A. Bracher, and L. Nerger (2019), Assimilation of global total chlorophyll oc-cci data and its impact on individual phytoplankton fields, *Journal of Geophysical Research: Oceans*, *124*(1), 470–490.

Raghukumar, K., C. A. Edwards, N. L. Goebel, G. Broquet, M. Veneziani, A. M. Moore, and J. P. Zehr (2015), Impact of assimilating physical oceanographic data on modeled ecosystem dynamics in the california current system, *Progress in Oceanography*, *138*, 546–558.

Sathyendranath, S., R. J. Brewin, C. Brockmann, V. Brotas, B. Calton, A. Chuprin, P. Cipollini, A. B. Couto, J. Dingle, R. Doerffer, et al. (2019), An ocean-colour time series for use in climate studies: The experience of the ocean-colour climate change initiative (oc-cci), *Sensors*, *19*(19), 4285.

Shulman, I., S. Frolov, S. Anderson, B. Penta, R. Gould, P. Sakalaukus, and S. Ladner (2013), Impact of bio-optical data assimilation on short-term coupled physical, bio-optical model predictions, *Journal of Geophysical Research: Oceans*, *118*(4), 2215–2230.

Siddorn, J., and R. Furner (2013), An analytical stretching function that combines the best attributes of geopotential and terrain-following vertical coordinates, *Ocean Modelling*, *66*, 1–13.

Skákala, J., D. Ford, R. J. Brewin, R. McEwan, S. Kay, B. Taylor, L. de Mora, and S. Ciavatta (2018), The assimilation of phytoplankton functional types for operational forecasting in the northwest european shelf, *Journal of Geophysical Research: Oceans*, *123*(8), 5230–5247.

Skákala, J., J. Bruggeman, R. J. Brewin, D. A. Ford, and S. Ciavatta (2020), Improved representation of underwater light field and its impact on ecosystem dynamics: a study in the north sea, *Journal of Geophysical Research: Oceans*, p. e2020JC016122.

Smyth, T. J., I. Allen, A. Atkinson, J. T. Bruun, R. A. Harmer, R. D. Pingree, C. E. Widdicombe, and P. J. Somerfield (2014), Ocean net heat flux influences seasonal to interannual patterns of plankton abundance, *PloS one*, *9*(6).

Song, H., C. A. Edwards, A. M. Moore, and J. Fiechter (2016), Data assimilation in a coupled physical-biogeochemical model of the california current system using an incremental lognormal 4-dimensional variational approach: Part 3—assimilation in a realistic context using satellite and in situ observations, *Ocean Modelling*, *106*, 159–172.

Storkey, D., E. Blockley, R. Furner, C. Guiavarc'h, D. Lea, M. Martin, R. Barciela, A. Hines, P. Hyder, and J. Siddorn (2010), Forecasting the ocean state using nemo: The new foam system, *Journal of operational oceanography*, *3*(1), 3–15.

Swart, S., S. J. Thomalla, and P. Monteiro (2015), The seasonal cycle of mixed layer dynamics and phytoplankton biomass in the sub-antarctic zone: A high-resolution glider

1031 experiment, *Journal of Marine Systems*, *147*, 103–115.
1032 Telszewski, M., A. Palacz, and A. Fischer (2018), Biogeochemical in situ observations–
1033 motivation, status, and new frontiers, *New Frontiers in Operational Oceanography*, pp.
1034 131–160.
1035 Torres, R., J. Allen, and F. Figueiras (2006), Sequential data assimilation in an upwelling
1036 influenced estuary, *Journal of Marine Systems*, *60*(3-4), 317–329.
1037 Triantafyllou, G., G. Korres, I. Hoteit, G. Petihakis, and A. Banks (2007), Assimilation of
1038 ocean colour data into a biogeochemical flux model of the eastern mediterranean sea.
1039 Vaquer-Sunyer, R., and C. M. Duarte (2008), Thresholds of hypoxia for marine biodiver-
1040 sity, *Proceedings of the National Academy of Sciences*, *105*(40), 15,452–15,457.
1041 Verdy, A., and M. Mazloff (2017), A data assimilating model for estimating s outhern o
1042 cean biogeochemistry, *Journal of Geophysical Research: Oceans*, *122*(9), 6968–6988.
1043 Visbeck, M., M. Araujo, A. Boetius, E. Buch, H. Claustre, T. Dabrowski, E. Delory,
1044 B. de Young, K. Drinkwater, A. Fischer, et al. (2015), More integrated and more sus-
1045 tainable atlantic ocean observing (atlantos), *CLIVAR Exchanges*, *67*(2), 18–20.
1046 Waniek, J. J. (2003), The role of physical forcing in initiation of spring blooms in the
1047 northeast atlantic, *Journal of Marine Systems*, *39*(1-2), 57–82.
1048 Waters, J., D. J. Lea, M. J. Martin, I. Mirouze, A. Weaver, and J. While (2015), Imple-
1049 menting a variational data assimilation system in an operational 1/4 degree global ocean
1050 model, *Quarterly Journal of the Royal Meteorological Society*, *141*(687), 333–349.
1051 While, J., K. Haines, and G. Smith (2010), A nutrient increment method for reducing bias
1052 in global biogeochemical models, *Journal of Geophysical Research: Oceans*, *115*(C10).
1053 Xing, X., H. Claustre, S. Blain, F. d'Ortenzio, D. Antoine, J. Ras, and C. Guinet (2012),
1054 Quenching correction for in vivo chlorophyll fluorescence acquired by autonomous plat-
1055 forms: A case study with instrumented elephant seals in the kerguelen region (southern
1056 ocean), *Limnology and Oceanography: Methods*, *10*(7), 483–495.
1057 Yu, L., K. Fennel, L. Bertino, M. El Gharamti, and K. R. Thompson (2018), Insights on
1058 multivariate updates of physical and biogeochemical ocean variables using an ensemble
1059 kalman filter and an idealized model of upwelling, *Ocean Modelling*, *126*, 13–28.